FLUID ABSORPTION SOLAR ENERGY RECEIVER

(Original Title was "Studies of Principles of Fluid Absorption Solar Energy Receivers")

FINAL REPORT

Principal Investigator: Dr. Edward J. Bair

Period of Contract: May 1, 1991 to April 15, 1993

Indiana University
P. O. Box 1847
Bloomington, IN 47402

Grant NAG3-1014

FLUID ABSORPTION SOLAR ENERGY RECEIVER

Edward J. Bair
Department of Chemistry
Indiana University
Bloomington, Indiana 47402

A conventional solar dynamic system transmits solar energy to the flowing fluid of a thermodynamic cycle through structures which contain the gas and thermal energy storage material. Such a heat transfer mechanism dictates that the structure operate at a higher temperature than the fluid. This investigation reports on a fluid absorption receiver where only a part of the solar energy is transmitted to the structure. The other part is absorbed directly by the fluid. By proportioning these two heat transfer paths the energy to the structure can preheat the fluid, while the energy absorbed directly by the fluid raises the fluid to its final working temperature. The surface temperatures need not exceed the output temperature of the fluid.

This makes the output temperature of the gas the maximum temperature in the system. The gas can have local maximum temperatures higher than the output working temperature. However local high temperatures are quickly equilibrated, and since the gas does not emit radiation, local high temperatures do not result in a radiative heat loss. Thermal radiation, thermal conductivity, and heat exchange with the gas all help equilibrate the surface temperature.

Potential advantages of the fluid absorption receiver

(1) It can deliver fluid at output temperatures up to the limit of thermal stability of the materials, and possibly higher, since it requires no additional temperature difference for heat transfer.

(2) It has a lower temperature thermal signature, with smaller energy losses for a given output fluid temperature.

Scope of the project

Scaling a solar receiver to a larger size is not a simple linear transformation. The project uses experiments on a small scale is to decrease the cost of developments on a larger scale by designing apparatus and experiments that validate a mathematical model applicable to a variety of detailed apparatus configurations. The progression of objectives is as follows.

Part I. Fluid absorption principles Identify the issues that determine the performance of a fluid absorption receiver and derive equations that quantify properties of receiver design that are generally applicable to the production of high temperature fluid, regardless of scale or application.

Part II. Laboratory receiver design Design and construct a small scale (0.5 kwatt) model receiver with the required geometry and fluid flow properties. Identify measurable properties that correlate the physical performance with the mathematical model in a way that facilitates scaling to greater power levels.

Part III. Laboratory receiver experiments Using simulated solar radiation, determine the contribution of specific processes to the relaxation toward a dynamic thermal steady state, and determine what changes in the receiver design will make it more nearly ideal.

Part IV. Field test receiver design Use the information from the laboratory receiver experiments to design a receiver operating at a higher power level (10-15 kwatt) of real solar radiation.

Part V. Field test experiments Test and develop the ability of the modeling procedure to predict performance on a larger scale.

Summary of Critical Issues Addressed

The receiver design must reconcile many interdependent issues by choosing numerical values for each of many variables. Once chosen and converted to hardware, only a very few variables are adjustable. Reconciling the issues is an iterative process having costs that escalate as the scale of fabricated hardware increases. The issues that have evolved during this study are outlined below.

1. Components and boundary conditions

The fluid output composition, temperature, pressure, flow rate, and return temperature depend on requirements of the application. Initially the application is simulated by a dummy load. These conditions are a somewhat arbitrary guess at what might prove to be useful. To be useful the capabilities of the receiver must be matched to the limitations of an application, such as mechanical and thermodynamic limitations on the efficiency of Brayton or Stirling cycle engines.

2. Collector-receiver optics

The total power, collection ratio, output aperture and solid angle, and tracking geometry of the collector must meet optical and mechanical specifications commensurate with a uniform temperature in the receiver cavity. The radiant power distribution at the input aperture, at the quartz window, and at the direct absorption surfaces are all critical in balancing the heat flux components.

3. Heat redistribution in the receiver

The temperature distribution in the receiver is determined by absorption of solar radiation followed by redistribution by thermal radiation, by thermal conductivity, and by convective exchange with the gas. To produce uniform temperature the heat redistribution must be analyzed by a point by point balance.

4. Fluid absorption

The fraction of the input radiant power absorbed by the fluid depends on the composition of the fluid, its spectral absorptivity in comparison with the solar spectrum, and the effective absorption path. The effective absorption path depends on the length of individual rays and variations in local gas density cause by localized absorption.

5. Heat transfer to the fluid

The limiting geometry of the direct absorption convective heat exchanger is specified by the flow cross section, heat exchange area, and heat exchange length. These can be related by 3 equations which include other fluid dynamic variables. Only a small range of heat exchanger geometries meet the boundary conditions for heat transfer to the fluid as well as uniform receiver temperature.

6. Heat transfer from the fluid to the simulated load

Heat transfer to the simulated load of a field test receiver must match the conditions for convective heat transfer to the fluid. The design of the heat sink heat exchanger and receiver heat exchanger are equally important for interpreting the test receiver performance.

7. Heat loss

Heat loss becomes easier to manage as the size of the receiver increases and surface/volume ratio decreases. Re-radiation loss decreases with increasing concentration ratio. In addition to delivering heat to the load, heat flow details are significant for limiting heat loss, for uniform temperature distribution, and for protecting heat sensitive components such as pressure seals.

8. Fluid circulation

The minimum compression ratio needed to provide mass flow and fluid velocity for convective heat exchange is much smaller than that needed for an efficient heat engine. In both cases the impeller and at least one bearing must operate at a temperature close to the return temperature of the fluid. The blower power efficiency is improved by integrating the flow path of the receiver with the flow path through the blower.

9. Materials problems

Bromine is highly corrosive, particularly at high temperature. Corrosion must be controlled to limit degradation of receiver materials and to limit loss or contamination of the fluid.

Quartz is subject to catastrophic failure due to mechanical stress, including thermally induced mechanical stress.

Current Status of the Development

Part I summarizes the quantitative basis for understanding the critical issues as they have evolved during the construction and partial testing of several versions of the small scale test apparatus and apparatus components.

Part II describes the design and construction of a small scale test apparatus that addresses the known issues that can be examined at this scale, and delineates those issues that can only be addressed using a larger scale. Two developments essential for a full operational test require the following steps for completion.
1) The surface of the gas bearing of the fluid pump must withstand bromine corrosion, high operating temperature, and galling on contact at low speed. Until the anti-corrosion surface is further developed to prevent galling, rotors can survive only a limited number of starts and stops. 2) A satisfactory seal must be found for a shaft turning at 10-15000 rpm under either vacuum or high pressure with minimum power loss.

Part III develops a mathematical model that calculates the time dependent temperatures of about 150 surface and volume elements as they evolve from a given initial condition to a steady state that is determined by the properties of the receiver and its inputs. Experimental measurements of the following aspects of the performance of the test apparatus are presented.

total radiant power input calibration
distribution of direct absorption power
distribution of fluid absorption power
input radiation loss by re-radiation
distribution of heat loss through the insulation
heat sink power calibration
gas flow velocity calibration
gas flow path in the receiver cavity

IV. After modification and verification the small scale model calculations can be adapted for use in both the design and testing of a larger scale (10-20 kw) field test apparatus

V. A field test would be designed for a particular solar collector facility, such as the facility at Sandia National Laboratories or the National Renewable Energy Laboratory.

SYMBOLS AND NOMENCLATURE[1]

Photometric properties[2]

Q	radiant energy, J	
Φ	radiant power, W	$\Phi = dQ/dt$
E	irradiance, W/cm^2	$E = d\Phi/dA$
I	radiant intensity, W/sr	$I = d\Phi/d\phi$
λ	wavelength	
σ_{SB}	Stefan-Boltzmann constant	5.67×10^{-12} W cm^{-2} T^{-4}
h	Planck constant	6.626×10^{-34} J/sec
c	speed of light	2.998×10^{10} cm/sec
ρ	reflectance	$\rho = \Phi_{ref}/\Phi$
τ	transmittance	$\tau = \Phi_{tr}/\Phi$
α	absorptance	$\alpha = \Phi_{abs}/\Phi$
ϵ	emissivity	$\epsilon = E/E_{bb}$
A	absorbance	$A = -\log_{10}\tau$
a	absorption coefficient	
m	molar concentration	

Solar properties[3]

x_{eo}	solar distance at earth orbit	$1.51 - 1.46 \times 10^{11}$ m
d_{sun}	solar diameter	1.82×10^{9} m
T_{sun}	surface temperature	6000 K
E_{sun}	surface irradiance	7.26×10^{4} kW/m^2
E_{eo}	irradiance at earth	1.32 - 1.41 kw/m^2
ϵ	subtended angle	.704 degrees

---

1. The symbols distinguish generic variables. Subscripts denote qualifiers for particular circumstances as defined in the accompanying text.

2. Photometric quantities refer to radiation over the spectrum. Terms for radiation in a particular spectral bandwidth are modified by a subscript. Irradiance refers to radiation emitted by a source, incident on a surface, or passing through a an area in space.

3. The values are consistent with a model in which the sun is a hot disc with the spectral irradiance of a 6000 K black body. Clear weather terrestrial values are typically about 68 % of the values in space.

Fluid dynamic properties[4]

x	cm	length
δx	cm	thickness
r	cm	radius
A_f	cm^2	flow cross section
A_h	cm^2	heat exchange area
d_f	cm	flow diameter
d_h	cm	hydraulic diameter
t	sec	time
T	K	temperature
P	atm	pressure
q	J	heat
P	J/sec	thermal power
M	g/mole	molecular weight
ρ	g/cc	density
C_p	J/mole-K	molar heat capacity
c_p	J/g-K	specific heat
vm	g/sec	mass flow rate
v_x	cm/sec	linear flow rate
κ	W/cm-K	thermal conductivity coefficient
η	g/cm-sec	viscosity coefficient
Re	$d_h \rho v_x / \eta$	Reynolds number
Pr	$c\eta/\kappa$	Prandtl number
Nu	$d_h h_c / \kappa$	Nusselt number
St	Nu/Pr-Re	Stanton number
h_c	W/cm^2-K	convective heat transfer coefficient

4. Usage is consistent with standard texts such as "Heat Transfer", by F. Kreith (international Press, Scranton Pa. 1958). Cases where the standard meaning of a symbol is not unique are to be distinguished from the context in which the symbol is used.

PART I. FLUID ABSORPTION PRINCIPLES

Objectives of part I

(1) Define temperatures which characterize a fluid absorption receiver.
(2) Specify the necessary components of a fluid absorption receiver system.
(3) Identify the issues that affect receiver performance.
(4) Derive mathematical conditions that are necessary and sufficient to correlate geometric and flow properties of the apparatus with heat transfer to the gas.
(5) Define a laboratory measurement strategy to maximize the predictive properties of a general model.

Part I outlines the critical issues that must be resolved to design a fluid absorption receiver, interpret experimental measurements, and change the design to a larger scale or different application. The parameters include variables of different kinds of heat transfer process, variables and constants of the working fluid, and variables and constants of the apparatus and its geometry.

Subsequent parts of the report apply these principles to experimental measurements which test and adjust the model, and test and adjust the utility of the model for scaling to larger size or different application. The object at each stage of experimental development is to identify and understand all processes whose quantitative characterization can be a critical issue in extrapolating to applications on a larger scale.

CONTENTS OF PART I

1. COMPONENTS AND BOUNDARY CONDITIONS

Temperature boundary conditions

In a fluid absorption receiver solar radiant power heats a stream of flowing gas to a high temperature, T_{max}, which transports the heat to a load and then returns to the receiver at temperature T_{min} with minimal temperature gradients and energy losses outside the load. Discussion of the receiver design is based on the following ideal performance.

1. Solid surfaces exposed to radiation are heated to a uniform high temperature, T_{max}, which is also the exit temperature of the gas.
2. Gas enters the receiver at temperature, T_{min}, and is pre-heated as it flows over surfaces maintained at T_{max}. In the preheat region T_{gas} remains well below T_{max} due to the inherent inefficiency of convective heat transfer.
3. Gas enters the fluid absorption region at temperature, $T_{gas} = T_{max} - \alpha(T_{max} - T_{min})$, where it absorbs a fraction, α, of the input radiation, raising its nominal temperature to T_{max}.

Receiver components

Fig. 1.1 shows the essential components of a fluid absorption receiver. The geometry and relative scale of the components depend on the size of the collector and the solar radiant power Φ_{tot} to the receiver. To deliver solar radiant power to the fluid efficiently a large number of issues must be addressed self consistently. The geometry of Fig. 1.1, which is only schematic, illustrates the major issues but has many possible variations.

The solar radiation collector is a parabolic reflector (not shown) that concentrates the radiation to an approximate image of the sun. A concentration ratio in the range 500-2000 is large enough to give the required receiver temperature and assure that the irradiance of the input radiation is large in comparison with thermal radiation out of the receiver. To deliver thermal power to a stationary facility the receiver design must accommodate the tracking motion of the collector with without using dynamic pressure seals outside the outer gas containment.

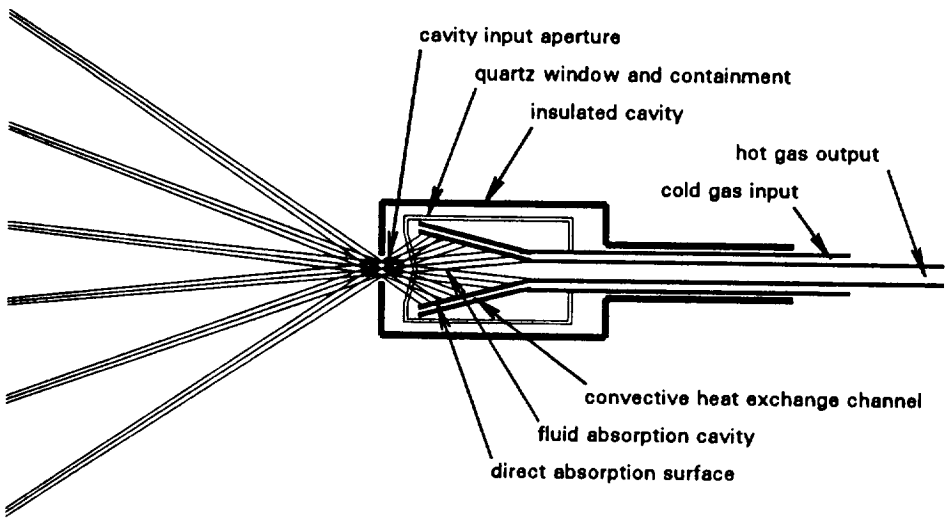

Fig. 1.1 Essential features of a fluid absorption receiver.

The **radiation shielding and radiation inlet aperture** isolates the receiver and hot gas delivery and return lines from the surroundings except for the radiation input. In a zero order approximation the receiver is a quasi-black body cavity with energy input through the radiation aperture and heat removal by the gas. For space applications the insulation consists of multi-layer radiation shields. Radiation loss through the inlet aperture is minimized by collector-receiver optics which make the irradiance at the input aperture from the collector large in comparison with the reverse irradiance from hot surfaces in the receiver cavity.

The **quartz window** at the front of the gas containment vessel transmits the concentrated solar radiation to the working fluid and the direct absorption surface. The window is displaced from the input aperture to reduce the irradiance at the window surface. In this diagram the window is an integral part of the containment, avoiding the problem of removing the containment seal from the high temperature environment. A concave window surface places the window surfaces normal to the diverging inlet radiation and improves the strength over a flat window.

The **direct absorption convective heat exchange surface** intercepts all of the input radiation that is not absorbed by the fluid. The objective is to balance the energy flux at each point on the surface due to radiation, conductivity, and convection, maintaining a

uniform temperature distribution at temperature T_{max}. This involves the following considerations. The irradiance input the at the direct absorption surface should have a uniform value roughly consistent with temperature T_{max}. The configuration of the area consistent with this irradiance must provide convective heat transfer $(1-\alpha)\ \Phi_{tot}$. In most designs the large flow cross section (and small convective heat transfer coefficient) in the fluid absorption region is likely to require that most of the convective heat transfer to the gas to occur in channels on the back side of that surface. The direct absorption and heat transfer surfaces must have high thermal conductivity.

The **closed loop gas circulation** passes the cold return gas over the direct absorption surface before entering the window area, where it is heated by fluid absorption. The degree to which the hot gas effluent and cold gas return are an integral part of the receiver, or a remote facility, depends on the application. The coaxial gas flow arrangement in Fig. 1.1 has the advantage of decreasing the insulation requirement by using the cold return gas as the primary insulation of the hot gas effluent. The blower may be external to the receiver cavity. If the hot gas is used to generate power, it may be an integral part of a turbine-compressor engine.

Heat redistribution model

During an experiment temperatures are measured at selected locations as a function of time as the system changes from an initial condition to an operating steady state. Whether or not the steady state temperatures of a test receiver satisfy the conditions that have been outlined, the object of the test is to account for the temperatures that are observed in terms of the balance of power at each point that can be attributed to known processes, primarily radiation, thermal conductivity of solids, and convective exchange between a solid surface and the gas. The power $P_{j,k}$ through contiguous elements with temperature $T_{j,k}$ and area $2\pi r_j \delta x_k$ or volume $2\pi r_j \delta r_j \delta xk$ is found by a coarse grained numerical integration, where r_j and x_k are the axial and radial positions, respectively. The rate of change in temperature of each element is related to the power at that element by

$$\rho\ V\ c_p\ dT_{j,k} = P_{j,k}\ dt \qquad (1.1)$$

where V, ρ, and c_p are the volume, specific heat, and density, ρ. The power through each element derived in the sections which follow.

For the solid surfaces

$$P_{j,k} = \int \Phi(\lambda)\, 10^{-a(\lambda)xm}\, d\lambda \qquad \text{direct absorption}$$

$$+ 2\pi r\delta x\, \sigma_{SB}\, (T_s^4 - T_{avg}^4) \qquad \text{thermal radiant power}$$

$$+ 2\pi r\delta x\, h_c (T_g - T_s) \qquad \text{convective exchange}$$

$$+ 2\pi r\delta x\, \kappa\, \Delta T_s/\partial r \qquad \text{radial conductivity}$$

$$+ 2\pi r\delta r\delta x\, \kappa\, (\partial^2 T_s/\partial x^2) \qquad \text{axial conductivity} \qquad (1.2a)$$

For the gas

$$P_{j,k} = \int \Phi(\lambda)\, [1 - 10^{-a(\lambda)\delta x\, m}]\, d\lambda \qquad \text{fluid absorption}$$

$$+ 2\pi r\delta x\, h_c\, (T_s - T_g) \qquad \text{convective exchange}$$

$$+ c_g\, v_m\, \Delta T_g \qquad \text{axial flow} \qquad (1.2b)$$

If the initial temperatures for the calculation are set as close to the steady state values, the calculation quickly finds steady state temperatures that agree with the assumptions of the calculation. Agreement between the calculated and observed temperatures is a necessary, but not sufficient, check on the validity of the calculation and its assumptions. In a first approximation the ideal receiver is a black body cavity with uniform temperature, T_{max}. This condition can be approximated without radiant power input by heating the receiver to T_{max} in a furnace, with and without the gas flow. This gives alternative checks on a part of the calculation using a reduced number of variables.

In an experiment the system is first heated to a steady state by the external furnace with the radiant power off. When the radiant power, Φ_{tot}, is turned on, the furnace power is reduced by the same amount. The residual power, if any, represent compensation for heat loss through the insulation.

2. COLLECTOR-RECEIVER OPTICS

The collector and the receiver are interdependent in several respects. The collector area determines the total radiant power input. The focal length determines the solid angle and collection ratio at the input aperture and the size of the input aperture. The collector configuration not only determines the mechanical tracking requirements, but has a major effect on the radiant power distribution at points beyond the nominal focus. The radiant power distribution at the receiver surface is calculated by a ray tracing procedure.

The power distribution is calculated by tracing the radiation to its origin at the sun. Each point on the collector receives a bundle of solar rays in an angle ϵ encompassing the extreme rays from the solar disk. The irradiance at any point along the optical path beyond the collector is a convolution of the irradiance at the points of origin in the solar disk with the irradiance at the points of origin on the collector. Optical surface errors and average pointing errors are added to the model by using a value for the angle ϵ greater than the true angle subtended by the sun.

Collector-Receiver configuration

The collector cross section normal to the solar radiation determines the total solar radiant power. The ratio of the effective focal length of the collector to its radius, f_c/r_{max}, determines the irradiance at the solar image as well as the acceptance angle of rays entering the receiver cavity and diverging toward the direct absorption surfaces. A large angle gives a small input aperture area and correspondingly large concentration ratio. This is the requirement for minimum re-radiation loss. The entry solid angle is the primary factor in matching the direct absorption surface to the geometry of the incoming rays to give uniform irradiance at the convective heat exchange surface. A small angle increases the depth over which energy is deposited on the receiver surface.

To avoid flexible connections in lines carrying fluid at high temperature, high pressure, and fast flow rates some applications require a fixed receiver. The collector must then rotate on a fixed axis to track the sun. Fig. 1.2 compares two configurations that accomplish this.

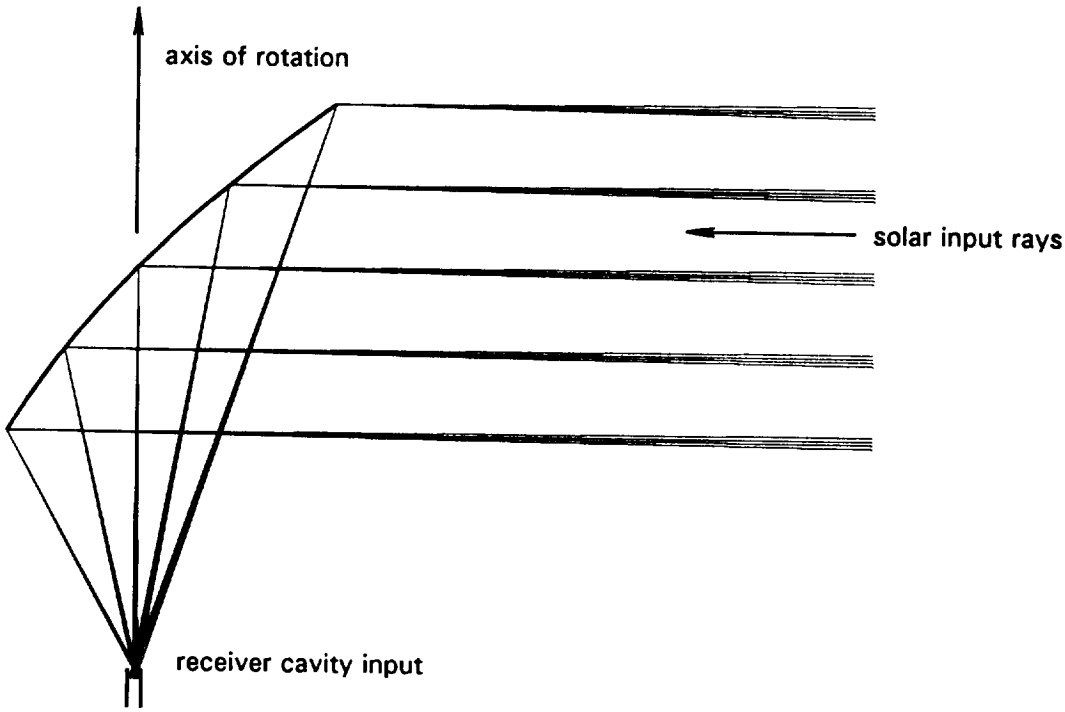

Fig. 1.2a Collector-receiver configuration using a 90° off-axis parabolic collector which tracks the sun by rotating on the same axis as the receiver.

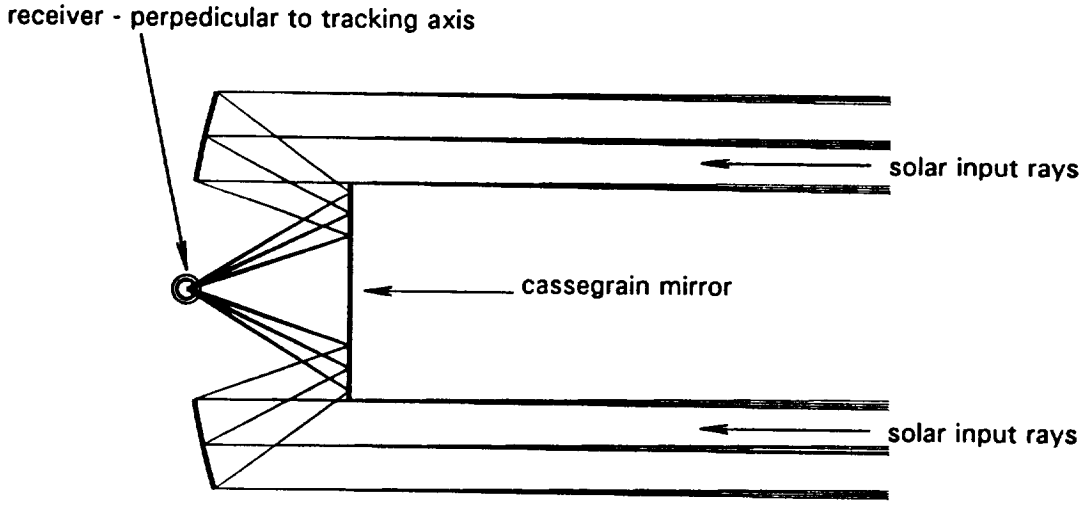

Fig. 1.2b Collector-Receiver configuration with parabolic collector and cassegrain secondary reflector which tracks the sun by rotating on an axis perpendicular to the rays entering the receiver.

The off-axis parabolic collector in Fig.1a tracks the sun by rotating about the axis of the receiver inlet. The maximum moment arm length is approximately r_{max}, the radius of the solar radiation cross section. The 45° angle requires a collector surface $\sqrt{2}$ times the cross section of the solar radiation. Radiation into the receiver cavity is nearly cylindrically symmetrical.

The cassegrain configuration in Fig. 1.2b locates the focal point at the origin of the parabola. The fraction of the solar cross section occupied by the cassegrain mirror is deceptively small. The parabolas in Figs. 1.2a and 1.2b b have the same solar cross section, and the total area encompassed by the two parabolas is also about the same. In the example shown the cassegrain intermediate reflector is a planar mirror located at half the focal distance of the parabola, in which case the ratio of the mirror diameters is $r_{min}/r_{max} = .55$. The maximum moment arm of the cassegrain system is approximately r_{max}, but a much larger fraction of the total assembly lies at the maximum lever arm length. Since the target surface in the receiver is perpendicular to the radiation input the input to a stationary receiver rotates with the collector. This complicates the receiver design. A nonplanar secondary mirror is a paraboloid with a significant quartic correction, $x = [y^2 - \frac{1}{4} y^4] [f_1 - f_2] / f_1 f_2$, where f_1 is the focal length of the primary mirror and f_2 is the focal length of the secondary. The diameter of a convex secondary mirror ($f_2 > f_1$) is smaller than a planar secondary. This increases the optical path and the solar image size and reduces the solid angle at the receiver and the concentration ratio. The minimum diameter of the secondary mirror is limited by its ability to radiate the heat it absorbs from the concentrated radiation from the primary.

Spatial distribution of radiant power input

In a first approximation the receiver is a black body cavity in which all surfaces have a uniform temperature, T_{max}. At $T_{max} = 1200$ K the black body irradiance inside the cavity is 11.8 watts/cm^2. The irradiance at the cavity opening to the collector must be much greater than 11.8 watts/cm^2 to minimize the re-radiation loss. The irradiance at the quartz window should not exceed about 50 watts/cm^2. Although thermal re-radiation helps to distribute the energy in the cavity, reasonably uniform radiant flux at direct absorption surfaces is necessary for a uniform temperature. The distribution of radiant power on a symmetrical direct absorption receiver surface is calculated as follows.

At the cross section of the beam reaching the collector the irradiance, E_{eo}, is uniform. The beam is directed toward the receiver in concentric cones whose cross sections form angles ϕ_{ij} with respect to the optical axis, as shown in Fig. 1.2a and Fig. 1.2b. Ray angles, ϕ_{ij}, from points on the surface of the primary parabola each have an i component, due to the slope of the parabola at radius, r_{ij}, and j component, due to the finite size of the sun encompassed by the angle ϵ, which is divided into j_{max} equally spaced components, $\Delta\epsilon_j$.

$$\phi_{ij} = 2 \tan^{-1}(\tfrac{1}{2} r^\circ_{ij}/f_1) + \Delta\epsilon_j \tag{2.1}$$

Radiant power leaving the collector is proportioned among i_{max} annular regions with area, $2\pi\, r^\circ_{ij}\, \Delta r^\circ$, each reflecting a bundle of rays in angle ϵ.

$$\Phi_{ij} = E_{eo}\, \alpha_j\, 2\pi\, r^\circ_{ij}\, \Delta r^\circ = \Phi_{tot}\, \alpha_j\, \beta_i \tag{2.2}$$

α_j is the fraction of the radiant power from a particular annular region of the solar disk. The angles in each ray bundle originate as the top or bottom of a set of $j_{max}/2$ annular rings of the solar disk, where $j = \pm 1$ to $\pm\, j_{max}/2$.

$$\alpha_j = \tfrac{1}{2}(2j-\tfrac{1}{2}) \sum_j (2j-\tfrac{1}{2}) \tag{2.3}$$

The radiant power from the annular area of the collector with a radius r°_{ij}, and width $\Delta r^\circ = (r_{max} - r_{min})/i_{max}$ is a fraction β_i of the total.

$$\beta_i = 2\pi\, r^\circ_{ij}\, \Delta r^\circ \,/\, \sum_i 2\pi\, r^\circ_{ij}\, \Delta r^\circ \tag{2.4}$$

In 3-dimensions, rays not altered by reflection or refraction are cones with radius r_i at the collector, and radius, r_{ij}, at distance, x_{ij}, from the nominal focal distance.

$$r_{ij} = r^\circ_{ij} + (f_1 - x_{ij}) \tan \phi_{ij} \tag{2.5}$$

Rays are traced through a reflecting or refracting surface by solving for the coordinates of the intersection of the ray with the surface, solving for the angle of the surface at that point, then changing the angle of the ray in accordance with Snell's law of reflection.

At the focal distance, the radial power distribution depends primarily on the j component of the angles, that is, the solar image. On moving away from the focal region, the distribution is increasingly dependent on the i component and develops a central minimum, corresponding to the central opening in the parabola, and two maxima on either side, due to the influence of the i and j on the distribution, respectively.
At any surface with axial symmetry, the irradiance is calculated as the irradiance of a set of k_{max} annular rings equally spaced at distances, x_k, along the surface of the receiver. The irradiance of each ring, E_k, is the sum of the radiant power of all rays Φ_{ij} which it overlaps.

$$E_k = \sum_i \sum_j \delta_{ij} \Phi_{ij}/\pi(r_k^2 - r_{k-1}^2) \tag{2.7}$$

where $\delta_{ij} = 1$ if $r_k \geq r_{ij} > r_k - \Delta r_k$, and otherwise $\delta_{ij} = 0$. At the large collector angle that must be used, optical aberrations make the cross section of the focal region far from a perfect solar image, regardless of the quality of the optics. For the purpose of concentrating the energy, the quality of the image is not an important criterion for optimizing the collector optics.

3. HEAT REDISTRIBUTION IN THE RECEIVER

The temperature distribution inside the receiver depends on the balance of heat flow at each element of the surface. A quantitative account requires a complete model calculation to find the steady state operating condition for a specific design. This would account for the distribution of the input radiant power from the collector, emission and absorption of thermal radiation, thermal conductivity of the receiver walls, convective exchange with the fluid, and heat loss through the insulation, through the input aperture, and by other parasitic flow paths. To formulate a test design it is useful to examine the relative magnitude of these processes.

Thermal radiation, described by the Stefan-Boltzmann law, is the dominant heat flow process at high temperature, except for the input itself.

$$P_{rad} = \sigma_{SB} \epsilon A T^4 \tag{3.1}$$

The Stefan-Boltzmann constant has a value $\sigma_{SB} = 5.67 \times 10^{-12}$ watts/cm^2-T$^{-1/4}$. For surfaces with emissivity $\epsilon = 1$ the thermal radiant power inside a receiver cavity at temperature 1200 K is 11.8 watts/cm^2.

Thermal conductivity of the receiver walls must also be large in order to heat the gas flowing on the back side of the receiver with no significant temperature difference. The radial conductivity of a cylindrical segment with length δx, radius r, and wall thickness $\delta r << r$ is as follows.

$$P_\kappa = \kappa \, 2\pi r \, \delta x \, \Delta T/\delta r \tag{3.2}$$

The thermal conductivity coefficient for 304 stainless steel is $\kappa = .3$ watt/cm-K, making the conductivity through a 3 mm (1/8 inch) wall thickness 1 watt/cm^2-K. The heat flowing to the back side of the receiver wall by thermal conductivity must total $P_\kappa = (1-\alpha) P_{tot}$ plus heat lost through the insulation. A large fraction of this heat is transferred to other surfaces of the heat exchanger, primarily by thermal radiation.

The rate of convective heat transfer to the fluid at the surfaces of the heat exchanger depends on the heat transfer coefficient, h_c, which in turn has a strong dependence on the flow conditions discussed further in section 1.5.

$$P_c = h_c A \Delta T \quad (3.3)$$

The temperature difference between the surfaces and the gas ranges from $T_{max} - T_{min}$ near the gas inlet to $T_{max} - T_{mid}$ at the receiver window. A typical value for the heat transfer coefficient, $h_c = .006$ watts/cm^2-K, gives $P_c = .5 - 2.0$ watts/cm$_2$. To obtain the required thermal conductivity through the receiver walls these numbers must be multiplied by the ratio of the heat exchange area to the area exposed to input radiation, roughly a factor of four, corresponding to a maximum temperature difference of less than 10 K between the inside and outside wall of the receiver at the gas input.

The primary factor affecting temperature uniformity in the receiver cavity is the local balance between solar radiant power and thermal radiation. Fig. 3.1a correlates the temperature unbalance that corresponds to the power unbalance at a particular surface element when the average thermal radiant power corresponds to 1200 K. The 4th power depenence on the temperature shows that small differences in heat flux can cause relatively large differences in temperature, particularly if the emissivity of the surface is small. Although this indicates that $\epsilon = 1$ gives the most uniform temperatures, the possibility that a higher reflectivity might aid in distributing the input radiation more uniformly must also be considered.

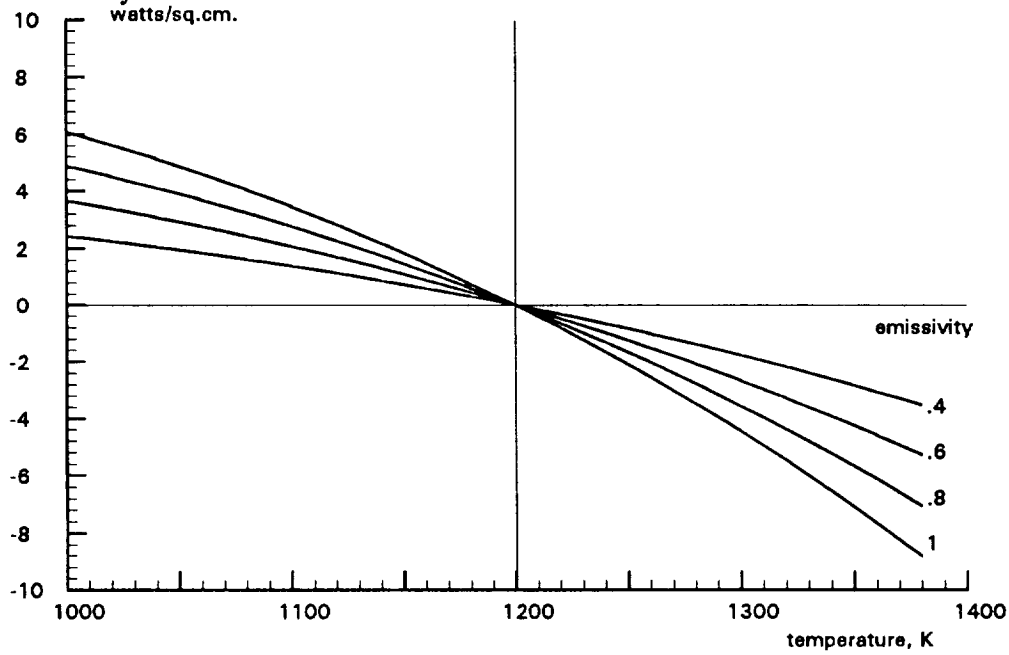

Fig. 1.3 Correlation between the radiant power unbalance and temperature deviation at a given surface element with thermal radiant power corresponding to 1200 K.

Heat loss through the insulation

When the walls of a cylinder are not thin, as is true for insulation, the implied derivative in equation (3.2) must be integrated between the inner and outer radii, r_i and r_0, to obtain the power as a function of the temperature difference between outer and inner surface.

$$P_\kappa = 2\pi x \kappa \Delta T / \ln(r_o/r_i) \tag{3.4}$$

By defining a logarithmic mean radius, $r_m = (r_o - r_i)/\ln(r_o/r_i)$, which is approximately equal to the mean radius if r_o and r_i are not too different, an area A_m at radius r_m reduces equation (3.4) to the form of equation (3.2). The thermal conductivity coefficient of good insulation is $\kappa = .001$ watts/cm-K. To limit the insulation loss to 5% requires a thickness $\delta x \approx 8.5\ r_m/r_{rec}$, where the ratio of mean insulation radius to the receiver radius makes this result independent of the scale of the receiver. For a large receiver where $r_m/r_{rec} \approx 1$ this condition is reasonable. For a very small receiver where $r_m/r_{rec} >> 1$ the required insulation thickness is not only unreasonably large, but the relative heat capacity of the insulation gives the system unreasonable thermal inertia.

Heat loss through the input aperture

The energy loss by a solar receiver surrounded by radiation shields has two principal origins, re-radiation through the input aperture and heat loss through the radiation shields. In the approximation that the inside of a solar receiver is a black body cavity at temperature, T_{max}, the power lost by re-radiation is $\Phi_{out} = \sigma A T_{max}^4$, where A is the area of the input aperture. The input power to the receiver through the same aperture is $\Phi_{in} = E_{eo} A_{col}$, where A_{col} is the collector cross section. The ratio gives the relative heat loss by re-radiation through the input aperture in terms of the concentration ratio of the collector, A_{col}/A.

$$\frac{\Phi_{out}}{\Phi_{in}} = \frac{\sigma T_{max}^4}{E_{eo}} \frac{A}{A_{col}} \tag{3.7}$$

For a receiver operating at $T_{max} = 1200$ K, reasonable efficiency requires a concentration ratio in the range 1600-2000. For fluid absorption receivers concentration ratios much higher than this are undesirable for the reasons discussed in section 2.

4. FLUID ABSORPTION

The fluid absorption component, Φ_{fluid}, and the direct absorption component, Φ_{dir}, are calculated by integrating the total radiant power of the sun, Φ_{tot}, appropriately modified by the transmittance of the gas over their respective wavelength dependences.

$$\Phi_{tot} = \int \Phi_{tot}(\lambda)\, d\lambda \tag{4.1}$$

$$\Phi_{dir} = \int \Phi_{tot}(\lambda)\, \tau(\lambda)\, d\lambda = (1-\alpha)\, \Phi_{tot} \tag{4.2}$$

$$\Phi_{fluid} = \int \Phi_{tot}(\lambda)\, [1-\tau(\lambda)]\, d\lambda = \alpha\, \Phi_{tot} \tag{4.3}$$

Absorption by halogens

The spectral absorptivities of halogen gases are shown in Fig. 1.4a. The spectral transmittance is $\tau(\lambda) = \log_{10}^{-1}(-a(\lambda)\, m\, x_{abs})$.

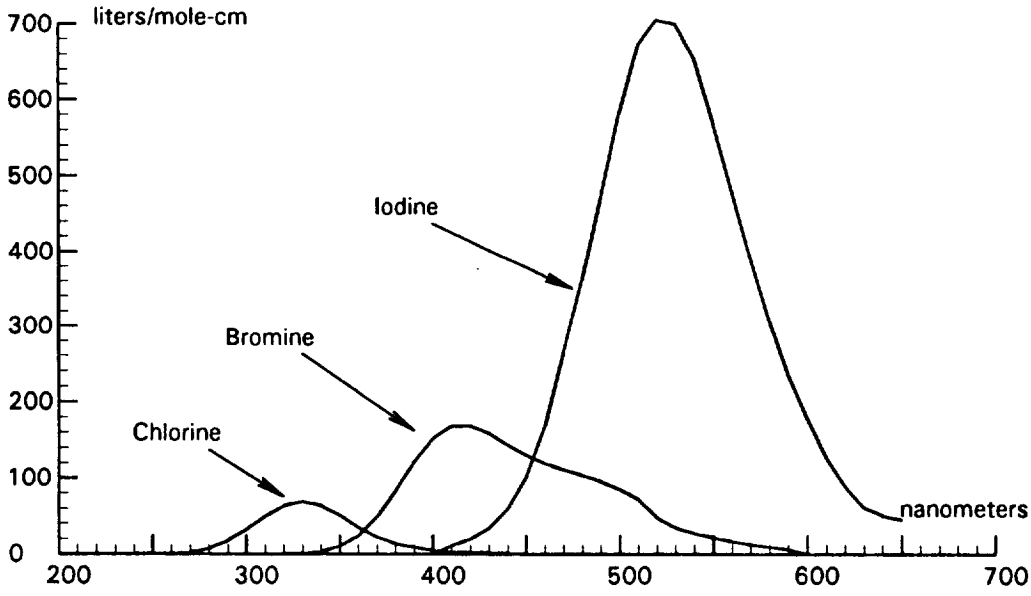

Fig. 1.4a Spectral absorptivities of halogen gases at 300 K.

Bromine absorptivity most nearly coincides with the peak of the solar spectrum. An path of about 1000 torr-cm of bromine absorbs most of the radiation that bromine can absorb, about 25-30 percent of the total. Although bromine forms a liquid at high partial pressure and low temperature, this should not be a significant issue in the planned operation.

Chlorine absorbs the solar radiation on the ultraviolet side of bromine. This amounts to about 5 percent of the total solar radiation, and would require about 2500 torr-cm of gas. The high concentration and possible complications due to mixing the gases make make the use of chlorine problematic.

Iodine is the strongest absorber. In combination with bromine a concentration of about 200 torr-cm of iodine would absorb about 10-15 percent of the radiation adjacent to the bromine spectrum on the long wavelength side, bringing the total to 35-40 percent. Iodine is a volatile solid which melts at 387 K and boils at 459 K.

There are two cautions about the using bromine-iodine mixtures. (1) No part of the gas containment can be allowed to reach a temperature where iodine condensation becomes a problem. (2) The distribution of gases among Br_2, I_2, and IBr under the conditions of this application is not known, and is not trivial to determine. The steady state composition is not necessarily the equilibrium thermodynamic composition. The spectrum of interhalogen gases in Fig. 1.4b suggests that degradation of absorber performance by the formation of IBr might be compensated by an increase in the original I_2 pressure.

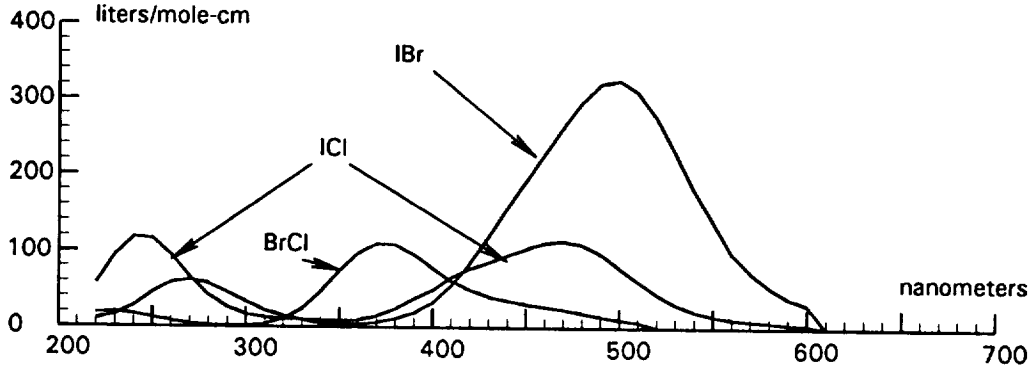

Fig. 1.4b. Spectral absorptivities of interhalogen gases at 300 K.

The gap in the center of the spectrum in Fig. 1.4c shows that the energy absorbed by bromine is α = .25-.30 of the total, depending on the concentration and path. Adding iodine, as shown in Fig. 1.4d, increases the fraction to α = .35-.40.

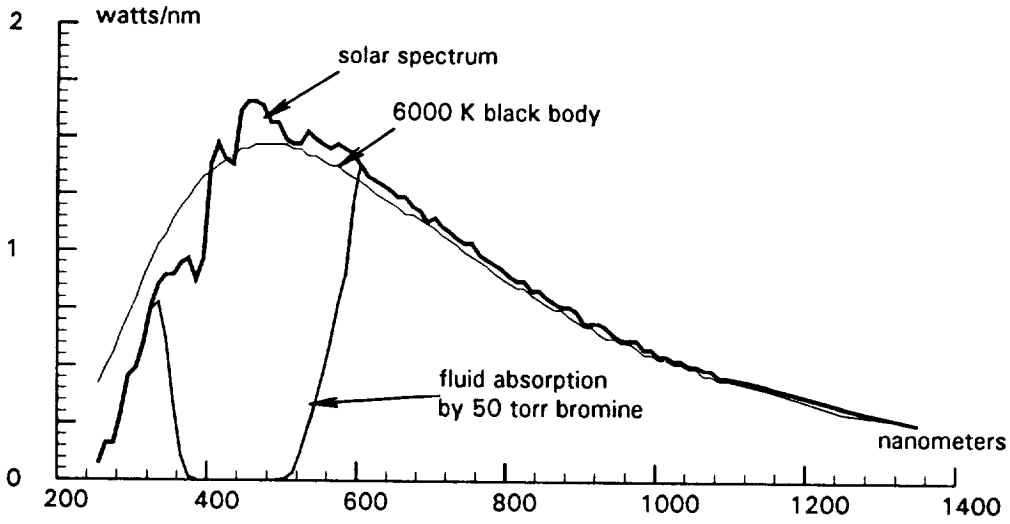

Fig. 1.4c. Fluid absorption component by a 10 cm path of bromine at 150 torr. The fraction of the solar radiant power absorbed is .280. Total radiant power 1 kW.

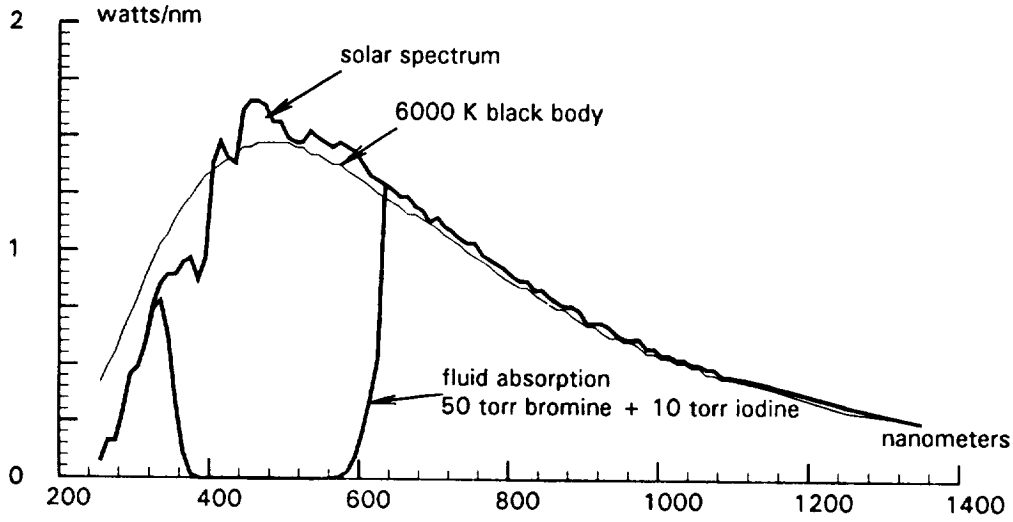

Fig. 1.4d. Fluid absorption component for a 10 cm path, 150 torr bromine, and 30 torr iodine. The fraction of the radiant power absorbed is .358. Total radiant power 1 kW.

Temperature dependence of the spectral absorptivity

At high temperature the population of higher vibrational states broadens continuous spectra. For example, the spectrum of chlorine in the v" = 1 excited state is nearly 80 percent broader than the spectrum of molecules in the v" = 0 ground state. The breadth of the absorptivity of molecules increases in still higher vibrational states. At temperatures in the range T_{min} to T_{max} only about 1/3 of the bromine molecules and only about 1/4 of the iodine molecules would be in the lowest vibrational state. Since the fluid absorption power given in Fig. 4.3 and Fig. 4.4 is on the molar absorptivities at 300 K, the fraction of the energy absorbed by the fluid deduced from these data is a lower limit. 50 percent fluid absorption might be a realistic upper limit.

Table 4.1 Relative populations of vibrational states at high temperature.

v	Bromine		Iodine		
	1000	1200	1000	1200	K
0	.367	.316	.261	.223	
1	.231	.215	.192	.173	
2	.146	.147	.142	.134	
3	.093	.101	.105	.104	
4	.038	.047	.077	.081	
5	.024	.033	.057	.063	

Fluid absorption geometry

In still gas with uniform density the increment of radiation absorbed per unit thickness of the gas decreases exponentially with distance from the window along each ray to the direct absorption surface with a different decay constant at each wavelength. The absorption increases the temperature of the gas element, decreasing its density and bromine concentration, and causing some flattening of the exponential decay. The density gradients are disrupted by flow. Equation 4.2 is probably adequate to estimate α, but not the distribution of the fluid absorption energy.

5. HEAT TRANSFER TO THE FLUID

Values for at least three independent variables are required to specify the geometry of surfaces that provide the minimum convective heat exchange for the required amount of heat. The following properties are chosen for the derivation that follows.

A_f	flow cross section
A_h	heat transfer area
x_h	heat transfer length

Limiting convective heat exchange geometry

When operating at a steady state the gas must deliver heat equal to the input radiant power, Φ_{tot} (minus losses), to the receiver load (heat sink).

$$\Phi_{tot} = v_m c_p (T_{max} - T_{min}) \tag{5.1}$$

A fraction, 1-α, of the total radiation absorbed by the receiver walls must be transferred to the gas by convection from surfaces with total area A_h. The heat transfer rate is proportional to the area and the temperature difference between the surface and the gas, the heat transfer coefficient, h_c being the proportionality constant. Since the gas temperature at the output of the convective heat exchanger, T_{mid}, is well below T_{max}, there is no appreciable error in using the arithmetic average temperature, $T_{avg} = \frac{1}{2} (T_{min} + T_{mid})$, where $T_{mid} = T_{min} + (1-\alpha)(T_{max} - T_{min})$.

$$\Phi_{dir} = A_h h_c (T_{max}-T_{avg}) = (1-\alpha) \Phi_{tot} \tag{5.2}$$

It is convenient to combine terms containing the temperature differences and the fraction absorbed by the fluid as a dimensionless constant, β. It has a value near one that depends on the fraction of the power absorbed by the fluid but is independent of the temperature differences.

$$\beta = (1-\alpha) (T_{max}- T_{min}) / (T_{max}- T_{avg}) = 2 (1-\alpha) / (1+\alpha) \tag{5.3}$$

These equations combine to give limits imposed by the input-output energy balance.

$$h_c = \frac{v_m c_p}{A_h} (1-\alpha) \frac{T_{max}- T_{min}}{T_{max}- T_{avg}} = \frac{v_m c_p}{A_h} \beta \tag{5.4}$$

The heat transfer coefficient is proportional to the Nusselt number which is roughly the inverse of the relative thickness of the boundary layer which insulates the heat exchange surfaces. The Nusselt number and the Reynolds number both increase with linear gas velocity with a complex interdependence that can be determined empirically. A large heat transfer coefficient requires a large Reynolds number, preferably in the turbulent flow regime. The limits imposed by fluid dynamics are given by the following expression which has been obtained for experimental data at velocities where Re $\geq$ 10,000.

$$Nu = 0.023 \, Pr \, Re^{0.8} \tag{5.5}$$

Substituting the required definitions in equation (5.6) gives the heat exchange coefficient in terms of the fluid dynamic variables.

$$h_c = .023 \frac{c_p}{A_f} \left(\frac{\eta A_h}{4 x_h} \right)^{0.2} v_m^{0.8} \tag{5.7}$$

Substituting this empirical definition of h_c into the heat balance equation (5.3) gives a relationship among the geometric variables, A_f, A_h, and x_h is obtained.

$$A_h^{1.2} = 57 \beta \left(\frac{v_m x_h}{\eta} \right)^{0.2} A_f \tag{5.8}$$

A more convenient set of equations is obtained by reintroducing the Reynolds number Re $= 4 v_m x_h / \eta A_h$. A third condition follows from the relation between mass and linear flow velocity.

$$A_h/A_f = 43 \beta \, Re^{0.2} \tag{5.10}$$

$$A_h/x_h = 4 v_m / \eta \, Re \tag{5.11}$$

$$v_m = \rho v_x A_f \tag{5.12}$$

Heat transport by forced convection

An important distinction between heat flow in solids and heat flow in fluids should be noted. The temperature of a solid refers to a volume element that is fixed in space containing a mass element that is also fixed in space. The temperature of fluid refers to a volume element in fixed laboratory coordinates that contains a succession of mass elements at different times. The convective flow differential describes the rate of change in temperature of whatever mass occupies the space at a given time.

$$dT/dt = \partial T/\partial t + v_x \partial T/\partial x \tag{5.13}$$

The first term is the component of temperature change in the mass element that currently occupies the specified volume element. It can be expressed as the sum of contributions by each heat exchange process affecting that element. The second term is the component of temperature change the volume element due to the mass transport through that element. The mass transport component of the energy flux through a given volume element, the difference between the power input and output, depends only on the input-output temperature difference in the approximation that c_p and v_m are constants.

$$P_m = c_p v_m \Delta T \tag{5.14}$$

Conservation of mass requires a constant mass flow rate at every point around the closed loop. Equation (5.14) distinguishes the last component of equation (1.2b) from the first two components.

6. HEAT TRANSFER FROM THE FLUID TO THE SIMULATED LOAD

The ultimate disposition of the heat is a water cooled heat sink which is calibrated as a calorimeter by measurements of the flow rate and the input-output temperature difference. Heat flow to the heat sink occurs in two steps, convective exchange between the gas and surfaces at a temperature T_{base}, and thermal conductivity from between those surfaces and the cooling water. The simulated load must be designed to distinguish heat carried out of the receiver by the gas from parasitic heat losses through alternative radiative and conductive paths.

Convective transfer from the gas

The heat balance conditions on the heat exchanger that absorbs the heat from the gas are similar to those for the direct absorption heat exchanger in the receiver. As in the receiver it is possible to define effective average temperatures that reduce the calculations to simple algebraic expressions.

$$\Phi_{tot} = v_m c_p (T_{max} - T_{min}) \tag{6.1}$$

$$\Phi_{tot} = A_h h_c (Tavg - T_{base}) \tag{6.2}$$

In this case T_{avg} is the median temperature of the gas between the exit and entrance of the receiver $T_{avg} = \frac{1}{2} (T_{min} + T_{mid})$. For convenience the temperature ratio is expressed as a quantity $\gamma = (T_{max} - T_{min}) / (Tavg - T_{base})$ which must have a value significantly less than one for the heat transfer to be complete, that is, $T_{base} << T_{min}$. In a steady state operation the value of T_{base} is determined by the balance between the convective heat transfer to the base and the conductivity between the base and the heat sink. In practice this relation will be complicated by parasitic heat loss. One of the functions of the design is to make these parasitic losses small. These equations combine to give the limits imposed by the input-output energy balance on the heat transfer coefficient. This is compared with the expression obtained previously for the heat transfer coefficient in terms of fluid dynamic quantities.

$$h_c = \gamma v_m c_p / A_h \tag{6.3}$$

$$h_c = .023 \frac{c_p}{A_f} \frac{\eta A_h}{4 x_h}^{0.2} v_m^{0.8} \quad (6.4)$$

Combining equations (6.3) and (6.4),

$$A_h^{1.2} = 57 \beta \frac{v_m x_h}{\eta}^{0.2} A_f \quad (6.5)$$

As before, this is converted to more convenient equations which linear dependence on the geometric variables by reintroducing the Reynolds number $Re = 4 v_m x_h/\eta A_h$. A third condition follows from the relation between mass and linear flow velocity.

$$A_h/A_f = 43 \gamma Re^{0.2} \quad (6.6)$$

$$A_h/x_h = 4 v_m / \eta Re \quad (6.7)$$

$$v_m = \rho v_x A_f \quad (6.8)$$

Heat sink temperature

The disposition of heat leaving the receiver is very much a function of the application. In a test receiver in which the heat is collected by a calibrated heat sink this disposition occurs as a series of steps of which convective transfer to the surroundings is only the first. In this discussion the convective heat transfer surroundings have be characterized by an effective temperature T_{base}.

The temperature T_{base} is the result of a balance between the convective exchange power heating these surfaces and processes that conduct the heat to the heat sink coolant. Although this is very much a function of the specific design, three general considerations are applicable.

1. The apparatus must be constructed to distinguish cleanly between heat transported to the heat sink and heat lost through the insulation and other parasitic losses.
2. One path to the heat sink begins with radiation through the quartz containment.
3. Another path is the thermal conductivity of the internal structures that support the surfaces represented by the temperature T_{base}.

7. GAS CIRCULATION

Gas circulation is an intrinsic part of the receiver design satisfied by a blower designed to match the flow impedance of the heat exchanger. The specifications include a mass flow rate that delivers thermal power output equal to the radiant power input, and a linear flow rate that meets the requirements for convective heat exchange. The flow is driven by external work done by the blower. The work must balance the viscous drag of the flow path, particularly the convective heat exchange section. Although the mass flow and pressure head are modest, specifications that satisfy both the mass flow and linear flow velocity requirements are narrow. In addition, the impeller and at least one bearing must operate at a temperature near T_{min}, and the blower geometry must be compatible with the receiver enclosure. Given a particular fluid absorption receiver containing the appropriate fluid, the only operating variable is the rotational speed of the blower. This section outlines the principles that are used to determine the specifications of the blower and to measure the effect of flow in the apparatus.

Flow measurement and interpretation

The model describes a gas flowing through a set of volume elements of fixed size. The mass flow velocity, v_m, along the flow path is constant, as required for conservation of mass. At the required mass flow rate the pressure differences and linear flow velocity, v_x, are small enough to satisfy the incompressible fluid approximation in which the gas density is independent of flow rate. (i.e., $v_x << $ mach 1 and $\Delta P/P < .07$) To interpret gas pressure measurements it is necessary to distinguish the hydrostatic pressure, static pressure, and stagnation pressure, and to distinguish between **average** and **local** temperatures and gas densities.

In a closed system the total number of moles is constant. The **hydrostatic pressure**, the pressure of the fluid at rest, is uniform but not necessarily constant. The temperature and gas density may change with location, k.

$$n = \sum_k n_k = P \sum_k V_k / RT_k \qquad (7.1)$$

The local gas density is obtained from the observed pressure and local temperature.

$$\rho_k = P M / RT_k \qquad (7.2)$$

Fluid flow creates pressure differences attributable to combinations of external work, viscous drag, and an apparent difference due to the bernoulli effect. The sum of the real pressure differences around a closed loop is zero. The mass flow rate is constant. The linear flow rate which determines the flow kinetic energy is inversely proportional to the local gas density and flow cross section, $v_x = v_m / \rho A_f$.

The **Bernoulli effect** is a decrease in the apparent local hydrostatic pressure which results because the pressure of a flowing gas is not isotropic. Flow causes a dynamic pressure difference equal to the macroscopic kinetic energy of the gas.[1] The observed pressure depends on the orientation of the probe with respect to the flow direction. A closed probe facing into the flow, such as a pitot tube, measures the **local stagnation pressure** or local thermodynamic pressure, the pressure associated with the local gas density.

Pressure in a flow stream is commonly measured by a probe orthogonal to the flow stream. This measures the local **static pressure** which differs from the stagnation pressure by the macroscopic flow kinetic energy of the gas.

$$P_{stagnation} = P_{static} + \tfrac{1}{2} \rho v_x^2 = P_{static} + \tfrac{1}{2} v_m^2 / \rho A_f^2 \qquad (7.3)$$

In a flow channel with no turbulence, viscous drag, or external work, energy is conserved and a change in the flow cross section causes a change in linear flow rate due to the exchange between potential and kinetic energy. The stagnation pressure, the static pressure plus the flow kinetic energy, is independent of the flow cross section and is the pressure that drives the flow. If the transition between flow cross sections is not smooth, macroscopic turbulence can cause the kinetic energy term to be smaller than predicted by the mass flow rate, the remainder being dissipated as heat.

---

[1] The thermodynamic internal energy function is the macroscopic potential energy due to the random kinetic energy of molecular motion. Gas flow uncouples the macroscopic kinetic energy in the flow direction from the random kinetic energy of molecular motion. According to the thermodynamic relation, $P = -(\partial E/\partial V)_S$, pressure is the potential energy per unit volume of the containment. Flow causes a decrease in the local static pressure (potential energy) equal to the kinetic energy of the flow.

Viscous drag is a the decrease in pressure in the flow direction that results from a loss of kinetic energy due to friction at the wall of a conduit. In a fluid absorption receiver the largest viscous drag component occurs in the convective heat exchange region. The shear stress at the walls is equal to the product of the kinetic energy of the gas, the wall surface area, A_h, and a skin friction coefficient, c_f. For turbulent flow the Blasius relationship, $c_f = .079\ Re^{-1/4}$, correctly accounts for the coefficient of viscosity in terms of the Reynolds number. The pressure required to move fluid through the pipe at velocity v_x is equal to the shear stress divided by the flow cross section.

$$\Delta P_{visc} = \tfrac{1}{2}\, c_f\, \rho\, v_x^2\, A_h/A_f = \tfrac{1}{2}\, v_m^2\, c_f\, A_h / \rho\, A_f^3 \qquad (7.4)$$

The **pressure head** that drives the gas flow is created by a compressor or blower and is equal and opposite to the total pressure difference due to viscous drag of the entire flow circuit. The flow restriction of the convective heat exchanger is the principal component of ΔP_{visc}. The pressure head is calculated in terms of the work done on the gas by the blower, ΔP_{work}, the work per unit volume. The function of the blower is to create pressure (energy per unit volume) in the form of flow velocity. The pressure head is dissipated in the system by converting the macroscopic kinetic energy of the gas to heat (random kinetic energy). Conversely, mechanical work can be extracted from the system by converting the kinetic energy of the gas to work done on the blades of a turbine.

PART II. LABORATORY RECEIVER DESIGN

Objectives of part II

Part II describes details of a small scale test receiver designed to minimize the cost of assessing the critical issues described in Part 1. The apparatus represents an evolution through several versions. Solar radiation is simulated by a 3 kwatt (electrical) xenon arc in an optical configuration that delivers approximately 0.5 kW of radiation at 55 watts/cm^2 opening. The apparatus has the following features.

- solar radiation simulated by a 3 kw xenon arc.
- axial cylindrical symmetry consistent with the model in Part I.
- quartz tube containment with flat quartz window.
- a blower to induce flow at 1-4 liters/sec.
- closed loop flow between the receiver and a heat sink.
- direct absorption and fluid absorption energy transfer in that sequence.
- instrumentation to measure variables defined by the model.

The simulated solar radiant energy is converted to heat of a stream of hot gas which flows to a calibrated heat sink. The target is a gas outlet temperature T_{max} = 1200 K with no surface temperatures higher than the output gas temperature. The heat transfer properties are measured as voltages from an array of thermocouples at points inside the receiver and pressure differences between points that characterize the flow rate. Surface temperatures are measured by thermocouples in mechanical contact with the walls. Gas temperatures are measured by fine wire thermocouples in the gas stream. Flow properties are measured by pressure differences at selected points.

The test receiver is designed to provide data to be compared in Part III with model calculations which yield steady state temperatures throughout the receiver as the end values of the relaxation from arbitrary initial temperatures. The experiments, the model calculations, and the receiver design are a part of an iterative procedure to reconcile observed and calculated results with the object of making the design procedure independent of scale.

CONTENTS OF PART II

1. SYSTEM OVERVIEW

Apparatus components

Fig. 2.1a is a schematic overview of the receiver and auxiliary apparatus. The test receiver is different from a real receiver both in scale and in the nature of the radiation source. It takes these difference into account in a way that makes the small scale tests a valid exploration of many aspects of a larger scale apparatus.

The **simulated solar radiation** from a Christie 3 kwatt (electrical) high pressure xenon lamp differs from solar radiation in two significant ways. The differences in spectral radiant power are discussed in Section 3. The xenon arc spectrum and the solar spectrum both approximate a 6000 K black body spectrum. Since the total power of even a large laboratory source is small, a simulated solar source must not only capture a large fraction of the total power. It must also concentrate the radiation to an irradiance approximating that of a solar point collector.

The **ellipsoidal collector** collects radiation through more than 3π steradians, unlike a solar collector which collects solar radiation from an infinitesimal solid angle. A simple ellipse cannot collect radiation through a wide solid angle and at the same time bring the beam to a sharp focus or large concentration ratio. With the xenon arc at one focus of the ellipse the beam is about 6" in diameter at the other focus.

The **non-imaging secondary cone** reduces the diameter of the beam by a factor of four, concentrating 640 radiant watts of the lamp's total output through a 3.8 cm diameter opening, an irradiance of 56 watts/cm^2 at the output of the cone. This corresponds to a solar receiver with a concentration ratio of about 560.

A heavy wall quartz tube with a flat quartz window at the front contains the receiver, the heat exchange gas, and the gas circulating blower. The tube is sealed by an aluminum end cap with a firm thermal connection to the heat sink. The end cap provides connections for evacuation and gas inlet, blower drive motor, and test probe outputs. The primary indicators of the receiver performance are the temperature and flow rate of the gas which circulates between the receiver and the circulating pump in the middle of the test apparatus.

Fig. 2.1a Overview of the .5 KW test facility

scale = 0.15 : 1.00

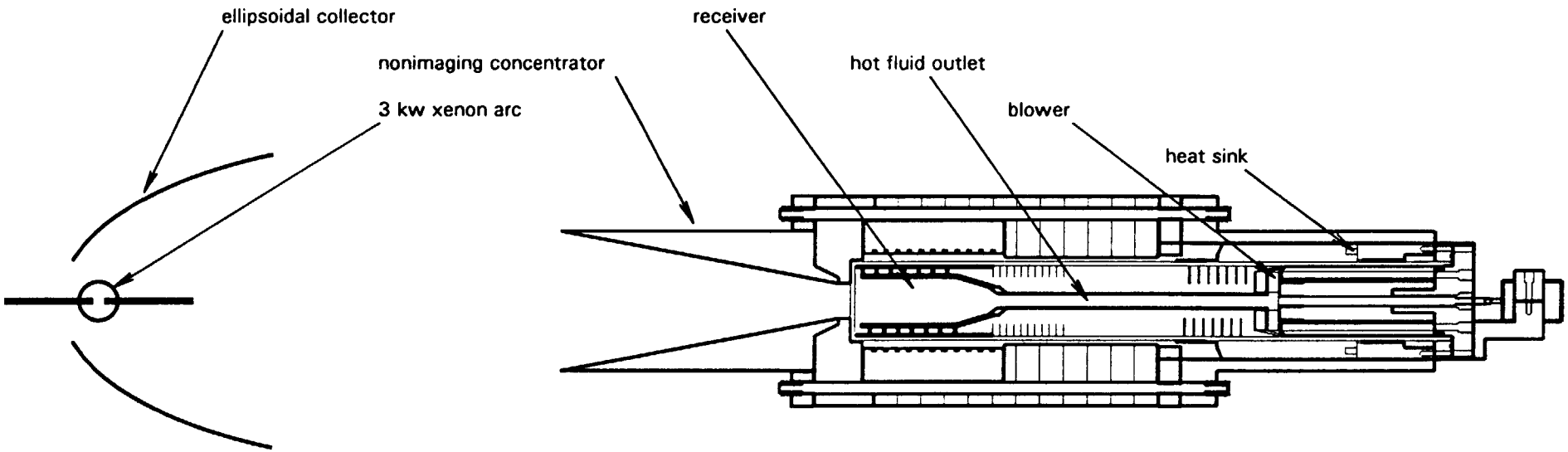

The receiver is a metal cylinder immediately behind the quartz window at the input aperture. The window end of the apparatus is insulated by a ceramic foam insulator. The sides are insulated with rings of insulator board. The outlet end of the receiver cavity is insulated from the heat sink section with radiation shields. This gives the receiver the optical properties of a black body cavity.

Radiant heating coils driven by a quantitative power source are used to counterbalance losses through the insulation. The absolute thickness of the insulation needed for a given temperature difference is independent of the diameter of the receiver. The thermal inertia of the insulation needed to reduce the losses from a small receiver to a small fraction of the total power input is too large. Temperature distribution measurements quantify the distribution of insulation heat losses that would otherwise occur.

The **water cooled heat sink** at the back end of the quartz tube is in solid thermal contact with the end cap of the quartz containment. It is maintained near ambient temperature with water flowing at a calibrated rate. Ideally the heat absorbed by the heat sink, as measured by the output-input cooling water temperature difference and flow rate, is equal to the solar radiant power input, Φ_{tot}. The practical delineation of heat sources and sinks requires the energy accounting described in Section 4.

Fig. 2.1b shows the internal components of the receiver in greater detail. The closed loop gas flow path is down the center of the receiver away from the window and toward the circulating blower. It leaves the receiver and enters the exit tube at temperature T_{max}. The centrifugal blower reverses the flow direction giving it a spiral velocity around the circumference of the enclosure. On leaving the blower the gas next passes through a heat exchanger in thermal contact with the blower at a temperature $T_b < T_{min}$, where it transfers energy to the surfaces of the blower and blower support column, leaving the receiver at temperature T_{min}. The gas then returns to the receiver through a spiral heat exchanger channel in the annular space outside the exit tube in which its temperature rises from T_{min} to T_{mid} as it reaches the radiation input window. In the vicinity of the window the bromine absorbs enough radiation to finish raising the temperature to an average value T_{max} as the gas completes the cycle. In a steady state the power flowing from the blower section to the heat sink exactly balances the radiant power input.

Fig. 2.1b Receiver / blower assembly

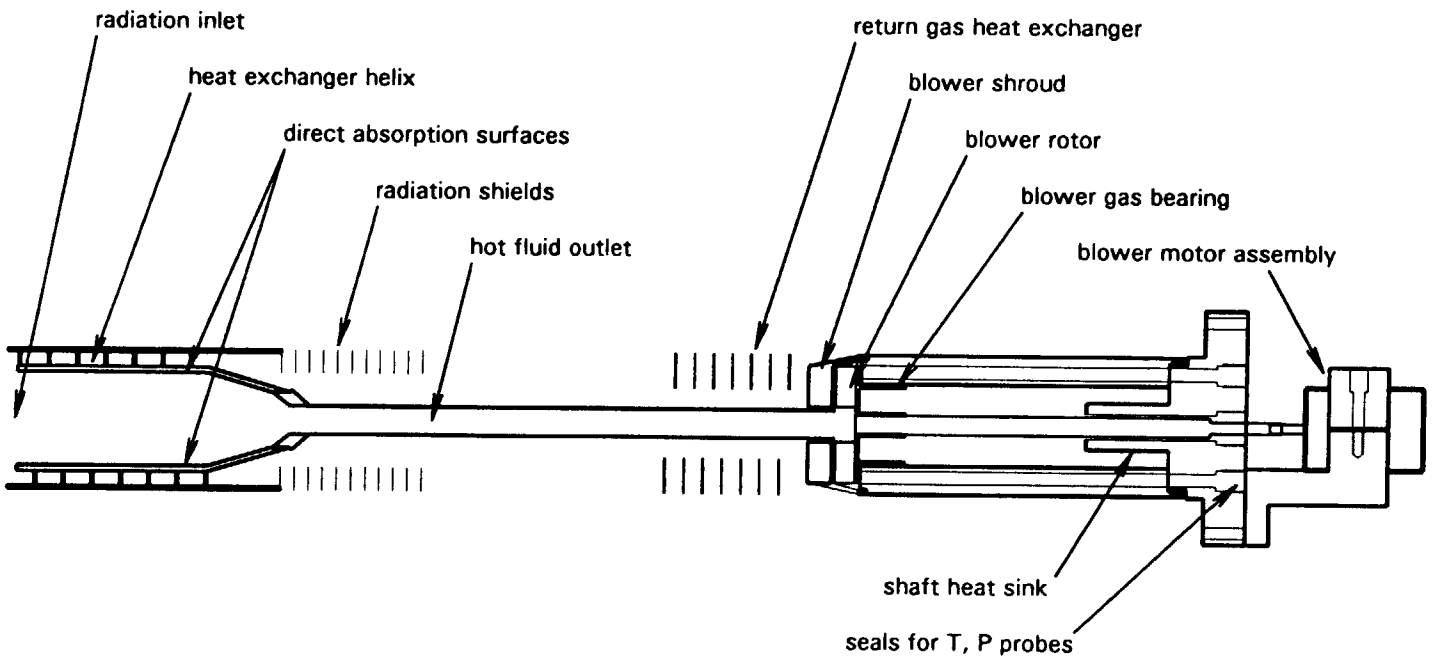

The **direct absorption surface** is a stainless steel tube with a diameter somewhat larger than the inlet aperture. The size of the tube is dictated by the surface irradiance and the minimum area required for convective heat transfer. The area shown has an average input surface irradiance of about 3 watts/cm^2 compared with the thermal irradiance of 11.7 watts/cm^2.

The **high temperature convective heat exchanger** on the back side of the direct absorption surface that is heated by radiation is a key element of the receiver design described in Section 4. Temperatures of the heat exchange surfaces are equilibrated thermal conductivity of the receiver wall and by radiative exchange within the channel, which is an order of magnitude faster than the convective exchange. The gas exits the heat exchanger in a cyclic path at the receiver window after a temperature gain T_{mid} - T_{min}, direct absorption component.

Fluid absorption adds an increment T_{max} - T_{mid} as the gas flows away from the window through the receiver to the exit tube. Convective exchange between the inside surfaces of the receiver and the gas is small, but not entirely negligible if the flow maintains a torroidal path.

A **centrifugal blower** driven by a dc motor circulates the gas through the system. The gas outlet from the receiver enters the central axis of a centrifugal rotor which reverses the overall flow direction. The gas flow out of the blower has a significant torque component which would normally be converted to pressure by a stator/diffuser. Instead the torque direction is matched to the helical path of the heat exchanger and is retained. The blower is designed to match linear flow rate, flow cross section, and pressure drop requirements of the heat exchange section. The blades and gas bearing surface are machined as a unit from stainless steel, then surface treated. By making the rotor, bearing, and shaft as light as possible, it is possible to satisfy the conditions under which the ambient gas is the only lubricant. The blower bearing is a heavy stainless steel column which also acts as a heat pipe to the heat sink.

The **low temperature convective heat exchanger** is in radiative contact with the heat sink as well as thermal contact with the blower support that transfers heat from the blower to the heat sink. The critical variable is the temperature of the heat exchanger and blower surfaces, $T_{base} < T_{min}$. Except for the uncertainties in defining the effective value of T_{base} the principles are similar to the high temperature heat exchanger.

Measurement Probes and Adjustments

The system is filled with the desired gas mixture using an MKS Baratron pressure gauge and sealed for the duration of an experiment. The pressure of the filled closed system, which increases in proportion to the average temperature according to the ideal gas law, $P = \rho_{avg} R T_{avg}/M$, is measured by a second high pressure MKS Baratron sensor. The system pressure is uniform except for small pressure drops across the compressor and across the heat exchanger due to the flow rate. The mass flow rate, v_m, is calibrated in terms of the rpm of the circulating pump as a separate experiment. The change in the pressure of the closed system reflects the average temperature of the gas. The local gas density, $\rho = MP/RT$, and local linear flow rate are calculated from measurements of the local gas temperature and flow geometry as the temperature is changed.

The motor rpm is sensed by an infrared tachometer and displayed continuously on the scale of a digital counter. The speed is adjusted by a precision voltage source to provide the required mass flow rate. The mass flow rate is measured in terms of the pressure difference between the input and output of the convective heat exchanger using a Omega type PX170 sensitive strain gauge sensor connected to an Omega series DP87 microprocessor controller and calibrated against a water manometer.

Heat delivered to the heat sink is measured by the cooling water flow rate and temperature increase. It is nominally equal to the radiant power input, but includes corrections for parasitic losses measured using the auxiliary heater with no gas flow. The auxiliary heater coil is controlled by an electronic powerstat whose output is continuously adjustable over a significant power range and is independent of the electrical characteristics of the load. The output of the auxiliary heater is calculated to compensate for all power that is not carried from receiver in the output gas.

Temperatures measured using type K thermocouples at 12-16 selected points in the gas and on the receiver wall are measured as a function of time. All temperature measurement information is processed by a special multi-channel amplifier and fed to an on-line computer which displays both the temperature distribution and the control information in real time. Locations at which temperatures are to be measured are mainly those required to verify and correct the power in the different heat flow channels described in the heat exchange design in section 4.

2. MATERIALS

Surface treated stainless steel

Most of the internal components of the receiver are made of type 304 stainless steel which has the advantage of strength, thermal stability, and availability in convenient forms. It has two disadvantages. Bromine corrodes the metal, particularly at high temperature, giving $FeBr_2$ and $FeBr_3$ vapor which condenses on the lower temperature parts of the apparatus. As a bearing surface for moving parts 304 stainless tends to gall or cold weld. Stainless steel therefore requires a surface treatment which permits the surface to serve as air bearings for the circulating pump and at the same time seals the surface against attack by bromine. Appendix 2.1 describes the development of an acceptable surface coating using various combinations of electropolishing, chrome plating, surface reaction with bromine at high temperature, and heat treatment.

Table 2.2a. Heat exchange properties of type 304 stainless steel

density, ρ	8.02 g/cm^3
specific heat, c_p	.577 J/g-K
thermal conductivity, κ	.30 W/cm-K
thermal expansion coefficient	12.0 x 10^{-6} K^{-1}
melting point	1700 K

Quartz

Quartz has high transmissivity throughout the main part of the solar spectrum at normal temperatures. It deteriorates by devitrification on prolonged exposure to temperatures above the annealing point and/or intense radiation. There is little information about the combination of high temperature and high irradiance on the rate of deterioration of the optical and mechanical properties. The threshold for damage by small diameter laser pulses is roughly 1000 J/cm^2 in 20 nsec pulses. The minimum requirement for a solar receiver is a continuous 60 watts/cm^2. The present judgement is that 1200 K is near the maximum of the temperature range at which the thermal and optical properties are stable for long periods of exposure before devitrification occurs.

Table 2.2b. Thermal properties of quartz

strain point[1], K	1266	
annealing point[2], K	1386	
softening point[3], K	1873	
thermal conductivity, W/cm-K	.022	1200 K
transmissivity (1 cm)	> .90	200 < λ < 3500 nm [4]
thermal expansion coeff, K^{-1}	.5 x 10^{-6}	
specific heat, J/g-K	1.1-1.5	300-1200 K
density g/cc	2.203	

[1] temperature below which thermal cycles leave no permanent strains.

[2] temperature at which thermal strains are removed in 10-30 min.

[3] temperature above which quartz is readily deformed.

[4] infrared cutoff increases from 2500 to 3500 mn when the manufacturing process (e.g., Corning 7957) prevents OH bands.

Argon and Bromine

Table 2.2c. Gas properties.

	argon	bromine
molecular weight, M g/mole	39.95	159.8
specific heat, c_p J/g-K	.262	.092
viscosity, η g/cm-sec	1.88x10^{-6}	2.23x10^{-6}

Ceramic insulation

Table 2.2d. Heat exchange properties of cotronix 360 ceramic board insulation

density, ρ	.256	g/cm^3
specific heat, c_p	1.046	J/g-K
thermal conductivity, κ	.00130	W/cm-K

Quartz containment and support structure

Aluminum is chosen for the heat sink and support elements in Fig. 2.2 due to its high thermal conductivity and satisfactory resistance to corrosion by bromine at room temperature. The quartz tube is sealed to the aluminum flange with a ring of epoxy cement approximately 1" wide. Two factors must be addressed. The rigid epoxy seal is a stress point in the mechanical structure. The connection between the quartz and the aluminum is a key element of the heat flow to the heat sink.

If the apparatus is supported by the quartz tube, the epoxy seal is subjected to a large force/cm^2 due to the weight and moment arm of the other components, including the end cap, and the unsupported weight of all components attached to the end cap. If the apparatus is supported by the end cap, the epoxy seal is subjected to large force/cm^2 due to the weight and moment arm of the quartz tube. Even if these forces are within the mechanical tolerance of the quartz at the point of the seal, it is easy to exceed the tolerance while the apparatus is being assembled.

Due to the difference in coefficient of thermal expansion, any significant temperature difference between the quartz and the aluminum creates enough thermal stress to break the quartz. On the other hand, the large difference in coefficient of thermal conductivity is a natural source of a temperature difference at the junction.

The aluminum support is a rigid assembly of a front flange containing the heat sink coolant channel, a rear flange containing the epoxy seal to the quartz and an o-ring seal to the end cap, and the end cap to which the other parts of the receiver are attached. The front and rear flanges each have a ring of flexible fingers strong enough to bear weight, but flexible enough to relieve thermal stress. The assembled apparatus is supported by the insulation surrounding the heat sink flange.

All of the aluminum components are in good thermal as well as mechanical contact and form a high conductivity path to the heat sink. Both sets of flexible fingers are in good thermal contact with the quartz. The fingers on the front flange connect the low temperature convective heat exchanger to the heat sink and limit the temperature rise of the flange end of the quartz tube. The fingers on the rear flange are a thermal shunt that further equalizes the temperature of the end cap and quartz at the epoxy seal.

Fig. 2.2 Quartz cell support / heat sink assembly

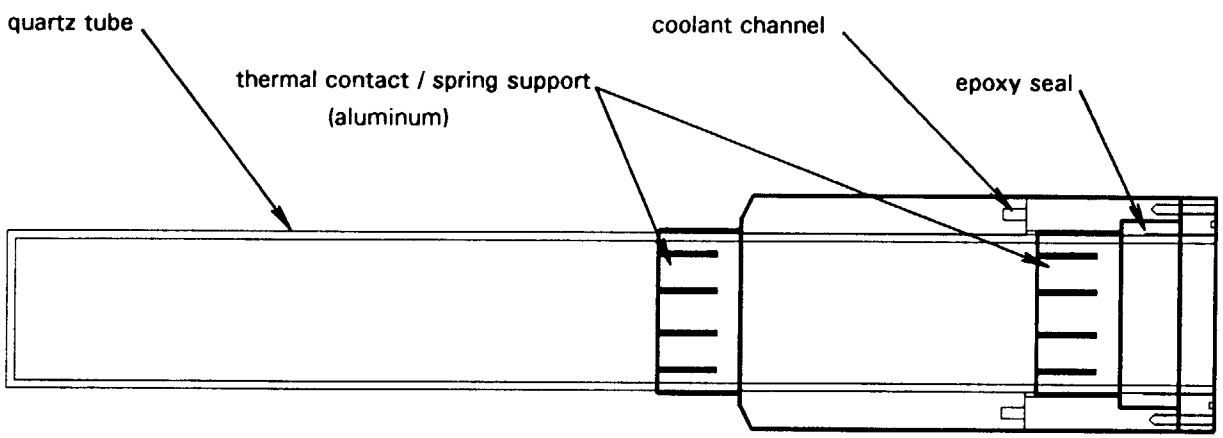

3. COLLECTION OPTICS

Xenon Radiation Source

The simulated solar radiation source, a Christie Model H30 xenon arc lamp, has a nominal electrical input power of 3 kw. The spectral radiant power of high power xenon arcs is compared with solar radiation and radiation by a 6000 K black body in Fig. 2.3a, using data from a report by C.A. Nicoletta (X-713-68-362, Goddard Space Flight Center). Except for the anomaly near 1-micron, the xenon arc and the sun both approximate a 6000 K black body. The xenon arc data in the figure are normalized to the observed total radiant power at the output of the collector optics, 640 watts. When the three sources are normalized to agree in the visible region of the spectrum the total radiant power of the sun and the 6000 K black body are about .71 times that of the xenon arc due to the intense infrared features in the 800-1050 nm region.

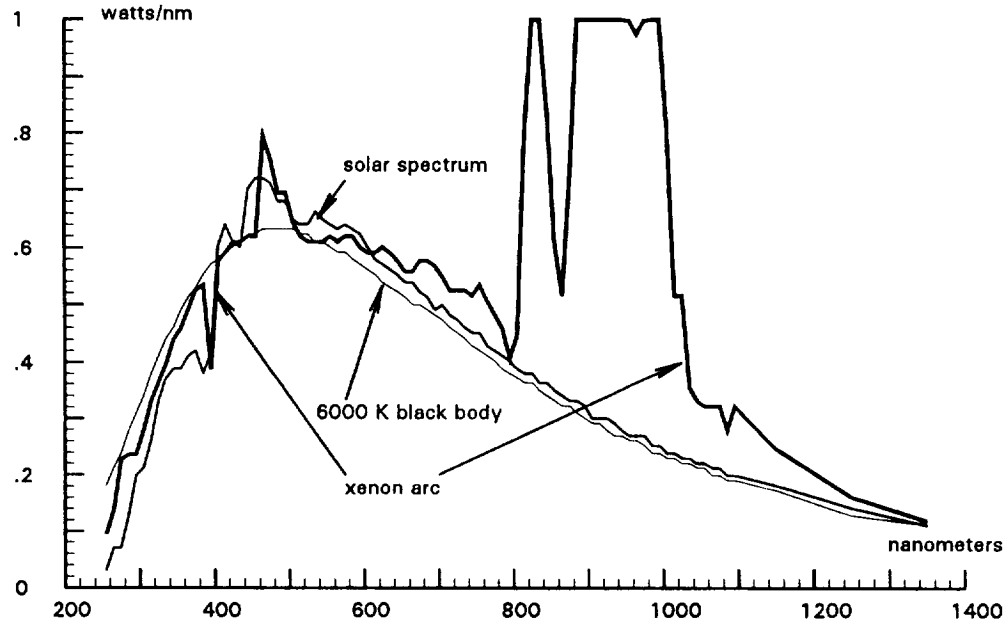

Fig. 2.3a Spectral radiant power of a xenon arc lamp compared with the sun and with a 6000 K black body radiator. Data for the xenon arc are normalized to the total radiant power deliver by the collection optics, 640 watts.

Concentrator optics

The ellipsoidal reflector in Fig. 2.1a is the primary concentrator. It has semi-major and semi- minor axes of 40.6 cm and 17.8 cm, respectively, placing the nominal foci 73.2 cm apart. The ellipse wraps around the source through an angle of about 3π steradians. It concentrates approximately 1500 watts of radiant power into an output beam 15 cm in diameter at the nominal focal distance.

A non-imaging secondary cone further concentrates the radiation to a diameter of 3.8 cm. The cone angle, $\beta = 10.5°$with respect to the axis, is roughly the angle from the edge of the ellipse to the nominal focus. A ray that enters the cone at angle α with respect to the optical axis is reflected from the cone at an angle $\alpha + 2n\beta$ after n reflections. If $\alpha + 2n\beta > \pi/2$, the ray is reflected back out of the cone. The cone thus increases the angular aperture as it increases the irradiance of light passing through the opening at the apex of the cone. The cone increases the output irradiance by roughly a factor of 6.5 at a cost of less than a factor of 3 in total radiant power.

Fluid absorption

The radiation is factored into direct absorption and fluid absorption components as described in Part I by numerical integration of the spectral radiant power of the xenon arc through bromine gas with measured transmittance, $\tau(\lambda) = -\log_{10}^{-1} [a(\lambda)\ m(Br)\ x]$. Due to the infrared spike in the xenon arc spectrum near 900 nm, the fraction of the radiation that can be absorbed by bromine is limited to about 19 percent, as illustrated in Fig. 2.3b.

$$\Phi_{xe} = \int \Phi_{xe}(\lambda)\, d\lambda \qquad \text{total radiation} \qquad (2.2)$$

$$\Phi_{dir} = \int \Phi_{xe}(\lambda)\, \tau(\lambda)\, d\lambda \qquad \text{direct absorption} \qquad (2.3)$$

$$\Phi_{fluid} = \int \Phi_{xe}(\lambda)\, [1-\tau(\lambda)]\, d\lambda \qquad \text{fluid absorption} \qquad (2.4)$$

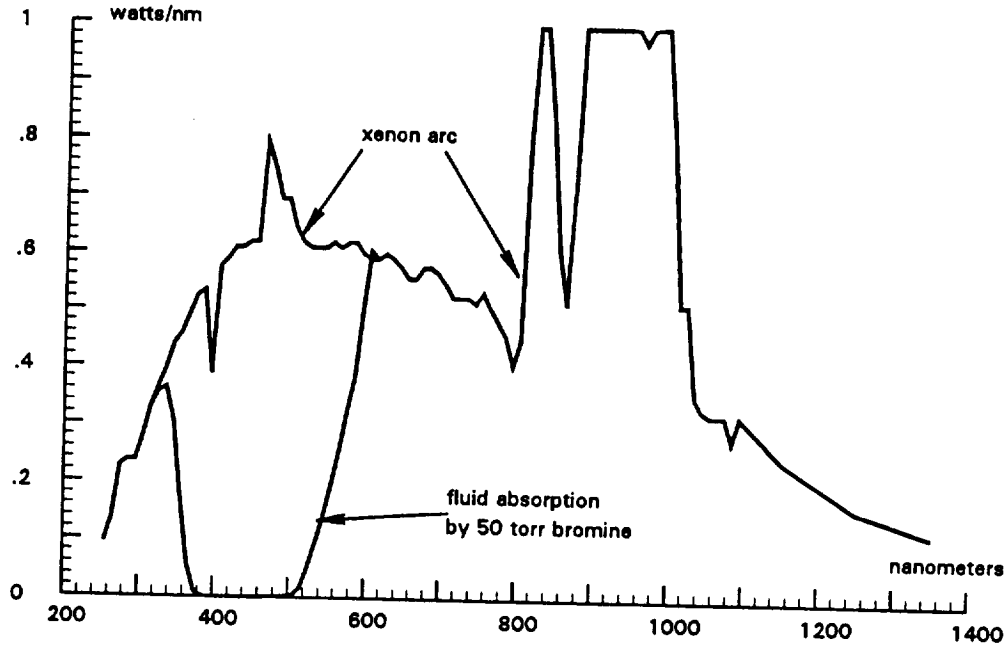

Fig. 2.3b Spectral radiant power of a xenon arc lamp normalized to 640 watt total radiant power showing the fraction of the radiation absorbed by 500 torr-cm of bromine.

Fluid absorption distribution

Although the above equations are adequate to estimate the fraction of the radiation absorbed by the fluid, the model calculations use a more detailed account of the distribution of absorbed power. The input power is divided into rays with varying depths of penetration into the receiver which can be measured by the distribution of direct absoption power. The absorption along any ray is not a simple logarithmic function of distance because the absorbed power induces a proportionate change in the temperature of the gas, changing the local gas density and bromine concentration. These effects are taken into account by calibrations described in Part 3.

4. HEAT EXCHANGE

Ideally the receiver is a cavity with contents at a uniform temperature, T_{max}. Power continuously enters the cavity as radiation and leaves as hot gas or parasitic losses. Uniform temperature requires a point by point balance among input radiant power, redistribution by thermal radiation and thermal conductivity, and convective exchange with the gas. Balancing the different processes requires the model calculations in Part III at minimum. The individual requirements are as follows.

Radiation input and receiver size

The output of the non-imaging cone is 55 watts/cm^2. The small size of the apparatus causes inefficiencies in insulating the radiant energy entrance that reduce the radiation to about 44 watts/cm^2 passing through the window. When surfaces in the receiver reach a uniform quasi-black body temperature of 1200 K the irradiance is 11.7 watts/cm^2 regardless of the emissivity of the surfaces. The input irradiance at the direct absorption surfaces is to be balanced by convective exchange with the gas. The magnitude of this unbalance, 1-3 watts/cm^2, dictates the general size of the receiver. Accordingly the 500 watt receiver is contained in a quartz tube with an inside diameter, d_q = 7.7 cm. Since radiation leaves the non-imaging cone at a large angle, the window placed as close as possible to the effective focus, making its effective diameter 3.8 cm. Due to the relatively small concentration ratio the re-radiation loss is about 25%. Ideally the concentration ratio of the collector would be a factor of 2-4 larger, making the relative re-radiation loss correspondingly smaller in a larger scale apparatus.

Direct absorption convective heat exchanger

The minimum conditions that satisfy the convective heat exchange requirements were derived in section 1.5. Table 2.4a gives numerical values for underlying properties that are independent of the geometry and scale of the apparatus. The total pressure is limited by the strength of the quartz container. The fraction of the radiation absorbed by the gas is smaller than for solar source radiation to the infrared spike in the xenon arc spectrum. The Reynolds number for the flow is arbitrarily assigned a value near the minimum value for turbulent flow, Re = 10000. Larger scale receivers may tolerate higher Reynolds numbers.

Table 2.4a System properties of 500 watt fluid absorption receiver

fraction absorbed by gas, α	.20
temperature ratio, β	1.33
argon pressure, $P_{Ar\ atm}$ at 298 K[1]	1.11 atm
bromine pressure, P_{Br} atm at 298 K	.066 atm
specific heat, c_p	.461 J/g-K
gas density, ρ	.00220 g/cc
viscosity coefficient, η	.000532 g/cm-sec
thermal conductivity, κ	.000209 W/cm-K
Reynolds number, Re	10000
Prandtl number, Pr	1.17
Nusselt number, Nu	43

[1] The receiver is filled and sealed at 1 atm total pressure. The operating pressure of about 4 atm results from the temperature increase. The average gas density is constant, but the local density depends on the local temperature.

The radiant power input dictates the mass flow rate, $\Phi_{tot} = v_m c_p (T_{max} - T_{min})$, as well as the scale of the receiver. The convective heat transfer properties of any fluid absorption receiver are given in terms of these properties by the four variables A_h, A_f, x_h, and v_x. Equations for three ratios among these variables derived in Part I are repeated below for dimensions in cm. They leave one independent variable.

$$A_h/A_f = 43\ \beta\ Re^{0.2} = 360\ A_f \tag{2.1}$$

$$\frac{A_h}{x_h} = \frac{4\ v_m}{\eta\ Re} = 2.9 \tag{2.2}$$

$$v_x = v_m / \rho\ A_f = v_v / A_f = 1840 / A_f \tag{2.3}$$

Trial values of v_x are give values of A_f, A_h, and x_h compatible with the optical requirements. The heat exchange length and area are accommodated by channeling the flow across the surface. Velocities in the range v_x = 800 - 1500 cm/sec give reasonable combinations of A_f, A_h, and x_h. The dimensions in Table 2.4b use v_x = 1500 cm/sec.

Table 2.4b Flow and heat exchange geometry of the direct absorption heat exchanger.

mass flow rate, v_m	3.67 g/sec
linear flow rate, v_x	1500 cm/sec
flow cross section, A_f	1.10 cm^2
heat transfer area, A_h	611 cm^2
heat transfer length, x_h	144 cm
helical fin o.d.	7.30 cm
helical fin i.d.	5.72 cm
channel width, x_w	1.38 cm
number of turns of the helix, n_t	7.1

The required heat exchange channel length, x_h = 146 cm, is obtained using a helical barrier with width x_w that causes the flow path to spiral around the back side of the direct absorption surface. Radiative exchange equilibrates the four sides of the channel at temperature T_{max}. The heat exchange area is the product of the perimeter of the flow channel times the channel length, x_h. The barrier confines flow to the space between the inside diameter of the heat exchanger cover, d_c, and the outer diameter of the receiver, d_r. The heat exchange area is equal to the channel length times the wetted perimeter of the flow channel.

$$A_h = (2\, x_w + d_c - d_r)\, x_h \qquad (2.4)$$

The outer diameter of the heat exchanger is chosen, in part, to give the flow channel a roughly square aspect ratio. A wide channel could be divided into parallel channels as in a multiple lead screw. In this case a single lead spiral is indicated. The tangent of the pitch angle of the heat exchanger helix is $\tan \phi = x_w / \pi\, dr$, from which the length of the receiver covered by the heat exchange helix is $x_r = x_h \sin \phi$. Following the sequence suggested by the table, on assigning values for the linear velocity, v_x = 1500 cm/sec, mass flow rate, v_m = 3.62 g/sec, and flow cross section, A_f = 1.10 cm^2, this procedure yields the remaining values for the heat exchange geometry.

Heat flow to the heat sink

Components of heat flow to the heat sink are identified in Fig. 2.4a. For a given temperature difference the insulation thickness is constant, making adequate insulation of a small scale receiver out of scale with the receiver. As an alternative, heat loss by the test receiver is counterbalanced by heater coils driven by an additional quantitative power source. This anticipates a measurement strategy involving static measurements with the blower off and dynamic measurements with the blower on. The static power components are estimated in Table 2.4c for apparatus filled with gas and heated to the desired T_{max} with the blower off and no radiation input. The outside temperature of the insulation accounts for most of this heat loss. The remainder which flows to the heat sink as a parasitic component that should be counted as a heat loss.

Table 2.4c Estimated heat flow components with the blower off and no input radiation.

Heat loss to be compensated	T_{hot}	T_{cold}	watts
insulation side walls	1200	400	127.5
insulation front end	1200	400	78.6
retainer rods to front plate	1200	400	37.4
retainer rods to back barrier	700	310	8.0
gas outlet tube	1200	400	9.4
outlet radiation shield	1200	400	64.1
total heater input			325.0
Heat flow to blower	T_{hot}	T_{cold}	watts
gas	1200	900	0.0
gas outlet tube	1200	400	9.4
outlet radiation shield	1200	400	64.1
total			73.5
Heat flow to heat sink			
radiation to heat sink	400	310	20.6
rotor support column	400	310	49.2
rotor spindle	400	310	.6
quartz tube, axial	400	310	2.3
total			72.7

Fig. 2.4a Heat flow elements of the 500 watt receiver.

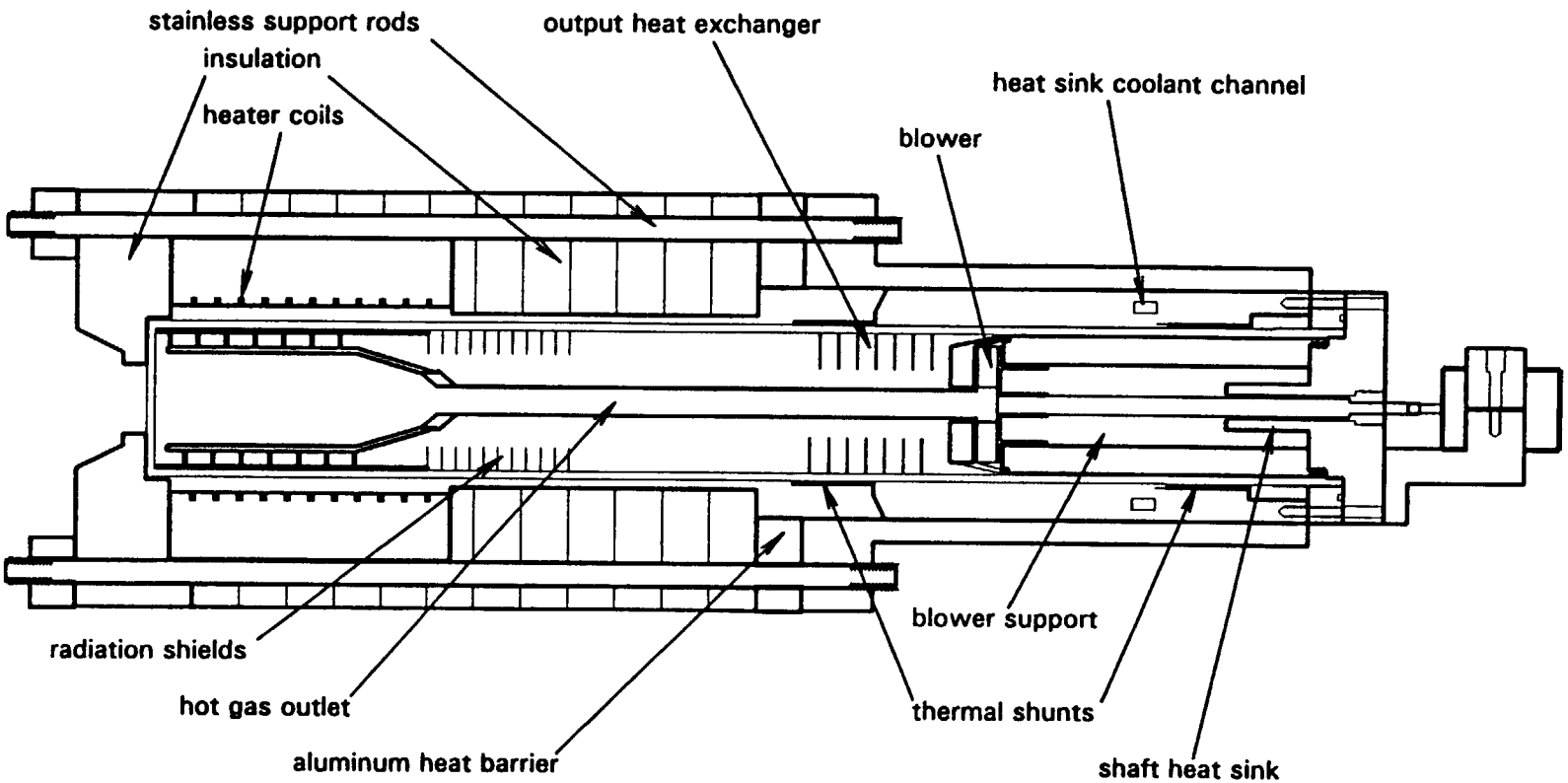

The temperature of the blower/heat exchanger region, T_{base}, results from a balance between the input and output to this region. In dynamic flow the input is mainly convective exchange with the hot gas. The output is divided between direct radiative exchange with the heat sink and thermal conductivity to the heat sink through the support for the gas circulation blower. The value of T_{base} is found by iterative adjustment of the sequence indicated by Tables 2.4c and 2.4d.

The dynamic power components estimated in Table 2.4d represent the case where the radiation is turned on and the blower rpm is adjusted until the receiver again reaches steady state operation at temperature T_{max}. The heat dynamic sink power is ideally the sum of the static heat sink power plus the radiant power input Φ_{tot}.

Table 2.4d Estimated heat flow components during dynamic operation with the blower and the radiation source on.

Heat loss to be compensated	T_{hot}	T_{cold}	watts
insulation side walls	1200	400	127.5
insulation front end	1200	400	78.6
retainer rods to front plate	1200	400	37.4
retainer rods to back barrier	700	310	8.0
gas outlet tube	1200	774	5.0
outlet radiation shield	1200	774	53.6
total heater input			310.1
Heat flow to blower			
gas	1200	900	500.0
gas outlet tube	1200	774	5.0
outlet radiation shield	1200	774	53.6
total with blower on			558.6
Heat flow to heat sink			
radiation to heat sink	774	310	288.7
rotor support column	774	310	253.7
rotor spindle	774	310	3.0
quartz tube, axial	774	310	11.8
total			557.2

Radiation shields together with the aluminum insulation barrier isolate the receiver from the heat sink. A set of 10 shields separate the cavity at temperature T_{max} from the low temperature heat sink at temperature T_{base}. Neglecting thermal conductivity through the gas, and assuming that each shield has the same reflectivity, ρ, the temperature difference between pairs of adjacent shields is proportional to the fourth power of the temperature. The power loss through a set of n shields follows from the fact that conservation of energy requires the same heat flow through each shield.

$$P = \sigma_{SB} A (1-\rho) (T_{max}^4 - T_{base}^4) / (n+1) \tag{2.5}$$

Direct radiation to the heat sink is the primary heat flow path connecting the low temperature heat exchanger to the heat sink. The principal uncertainty in estimating this power loss component is the effective area of the surfaces at T_{base} that radiate heat to the heat sink.

$$P = \sigma_{SB} A (1-\rho) T_{base}^4 \tag{2.6}$$

The blower support is a thick walled stainless steel cylinder attached firmly to the end cap. The thermal conductivity of 304 stainless is about an order of magnitude smaller than that of the aluminum end cap, but about two orders of magnitude larger than good insulation. This accommodates a significant temperature difference between the blower region and the end cap, at the same time allowing the required heat flow. The effective thermal length of the support can be trimmed by inserting an aluminum shunt as a thermal connection between cylinder and the rotor shaft heat sink.

Axial conductivity along the walls of the quartz container is less significant as a heat loss path than for the need to keep the epoxy seal to the end cap flange at room temperature. The quartz is attached to the end cap flange with epoxy cement strong enough to accommodate an internal cell pressure of about 5 atm. The low tolerance of the quartz-epoxy-aluminum seal to differential thermal expansion limits the temperature of the seal to 300 $\pm$ 40 K. To achieve this the heat flow through the quartz is short circuited to the end cap along the path through flexible aluminum fingers that contact the quartz in front of the epoxy seal. The nominal temperature at the thermal contacts, about 320 K results from a compromise which makes the fingers flexible enough to maintain firm contact with the quartz but heavy enough for good thermal conductivity.

Conductivity of the stainless steel rotor shaft is also significant less for the heat loss than for the need to keep the shaft seal near room temperature. The shaft rotates at high speed with one end at the blower temperature and the shaft pressure seal near room temperature. Conductivity is minimized by using thin walled stainless tubing. The shaft heat must be transferred convectively from the shaft through the gas surrounding it to the end cap. To facilitate this the rotor shaft is surrounded by a close fitting shaft heat sink The temperature gradient in the shaft lowers the temperature to about 350 K at the inside end of the rotor shaft heat sink. Inside the heat sink, which has a firm thermal connection to the end cap, a progressive fraction of the heat is transferred through the thin layer of gas surrounding. The heat transfer coefficient of the gas is calculated for a linear flow velocity equal to the speed of the rotor. The temperature at the pressure seal depends on the rate at which heat is transferred to the heat sink through the surrounding gas.

Heat sink convective heat exchanger

The temperature T_{base} calculated in Table 2.4d is used as the effective temperature of the heat sink convective heat exchanger. Using this plus the approximations used in deriving equations (6.6), (6.7), and (6.8) in Part I, the geometry in Table 2.4e gives the heat transfer which returns the gas to the receiver at temperature T_{min}.

Table 2.4e Flow and heat exchange geometry of the heat sink heat exchanger.

mass flow rate, v_m	3.67 g/sec
linear flow rate, v_x	1500 cm/sec
flow cross section, A_f	1.10 cm^2
heat transfer area, A_h	337 cm^2
heat transfer length, x_h	125 cm
helical channel o.d.	7.62 cm
helical channel i.d.	5.72 cm
channel width, x_w	1.16 cm
number of turns of the helix, n_t	6.0
overall heat exchanger length, cm	6.9 cm

5. GAS CIRCULATION

Blower design

Blowers function by subjecting a fluid to a macroscopic torque that is later converted to linear flow. Meeting both the flow specifications and the small size limitations of the small scale receiver is a challenge. When turbules of fluid in turbulent flow are not small in comparison with the flow channel through the blower the energy of the rotor can be dissipated by localized turbules whose microscopic torque does not contribute to the desired macroscopic output. The data in Table 2.4b show that convective heat exchange requires 1.5 liters/sec of gas through 1.5 m of a channel with 1.1 cm^2 cross section. The centrifugal blower in Fig. 2.5a is the best of several designs whose pressure head across the actual heat exchanger load was compared. The gas inlet and outlet are separated by a shroud that matches the of the rotor.

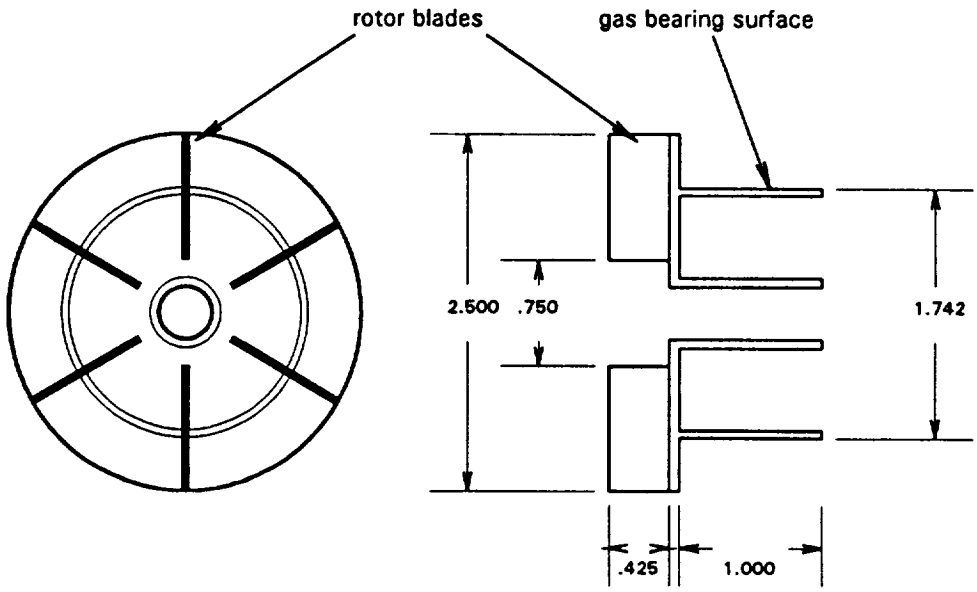

Fig. 2.5a Centrifugal rotor for the gas circulation blower.

The gas velocity and the pressure head depend on the tangential velocity of the rotor. A 15000 rpm dc permanent magnet motor provides a satisfactory margin above the required linear velocity of the gas. Straight blades performed marginally better than either forward or backward curving blades with the added advantage of easy machinability.

Ordinarily the shroud that separates the input and output flow streams would be in the form of stator (diffuser) vanes that direct the output gas in the desired path without doing work or dissipating energy. In the test receiver the circular path of the output gas is the desired direction for the low temperature heat exchanger. Turbulence losses are reduced simply by designing the heat exchanger paths as a continuation of the preferred helical flow direction. Pressure measurements show that the helical flow pattern persists through the fluid absorption chamber giving the gas a high linear flow rate and long path at the inside walls of the receiver even without vanes to guide it.

Centrifugal rotor bearing

As noted in Part I, significant problems are avoided if the bearings can be operated as gas bearings with the working fluid as the only lubricant. Meeting the design and criteria is primarily a matter of constructing the rotor to close tolerances with minimum mass. In this case the rotor must nevertheless be constructed of relatively high density stainless steel to meet the temperature and corrosion resistance criteria. Table 4.5b summarizes the minimum requirements for stable operation in the viscous flow regime according to Sommerfield's theory of lubrication. The Sommerfield criterion is met at roughly the speed for which the eccentricity is less than half the play. As a practical matter, the magnitude of the play must be large in comparison with the local dynamic deviations in the play dimensions. Lubrication by the ambient gas is not adequate for the rotor bearing in Fig. 2.5a at speeds below the calculated value. The observed regime of instability is passed as the speed of the motor exceeds about 4500 rpm, in reasonable agreement with the theory.

Table 2.5a. Minimum conditions for gas lubrication

$z = 1$	Sommerfield variable
$d = 1.742$ in	shaft diameter
$\ell = 1.00$ in	bearing length
$\delta = .010$ in	play
$\epsilon = .005$ cm	eccentricity
$m = 100$ g	shaft mass
$\eta = .00053$ g/cm-sec	viscosity coefficient of argon
$v_\phi = 2835$ rpm	shaft rotation rate

Blower drive and shaft seal

Initially the advantages of driving the blower by magnetic coupling through the walls of the containment appeared to be an attractive way to avoid the problems associated with a rotating seal. Although this may yet be reasonable technology for an actual receiver, the following problems require better solutions than the present effort was able to create.

1. Eddy current losses in the material that separates the driving and driven magnets dissipate excessive power, causing significant heating of the containment material, and reducing the effectiveness of the coupling. This problem was particularly severe in the present case because the end is made of aluminum. The problem is smaller in stainless steel which has smaller electrical conductivity, but a dielectric like quartz might be necessary for a satisfactory result.
2. Sufficiently strong magnets have large density and weight. The distribution of weight of the magnets that are available is not uniform. At the high rotational speeds that are necessary, this requires extremely careful dynamic balancing. The dynamic balance problem is discussed more fully in Appendix 4.2.
3. Although the corrosion resistance problem is greatly reduced because the driven magnet operates at room temperature, the coating procedure used for stainless steel is not directly applicable to the magnet material.

Although blower shafts driven by magnets were successfully dynamically balanced by the procedure in Appendix 4.2, an even better balance of a directly driven shaft was obtained simply by exercising extreme care in machining. Accordingly the blower was isolated using the teflon shaft seals in Fig. 2.5b which seal against both positive and negative pressure.

6. TEMPERATURE CONTROL AND MEASUREMENT

Multichannel temperature measurement

Thermocouple measurements are processed by an on-line computer which displays the temperature distribution and other control information in real time. The temperature distribution is measured by up to 16 thermocouples at representative points on the receiver walls and in the gas. The thermocouple outputs are conditioned by the computer interface in Fig. 2.6. It contains 16-parallel 2-stage amplifiers in a circuit designed to circumvent the problems that arise when many thermocouples are connected to a common conductor.

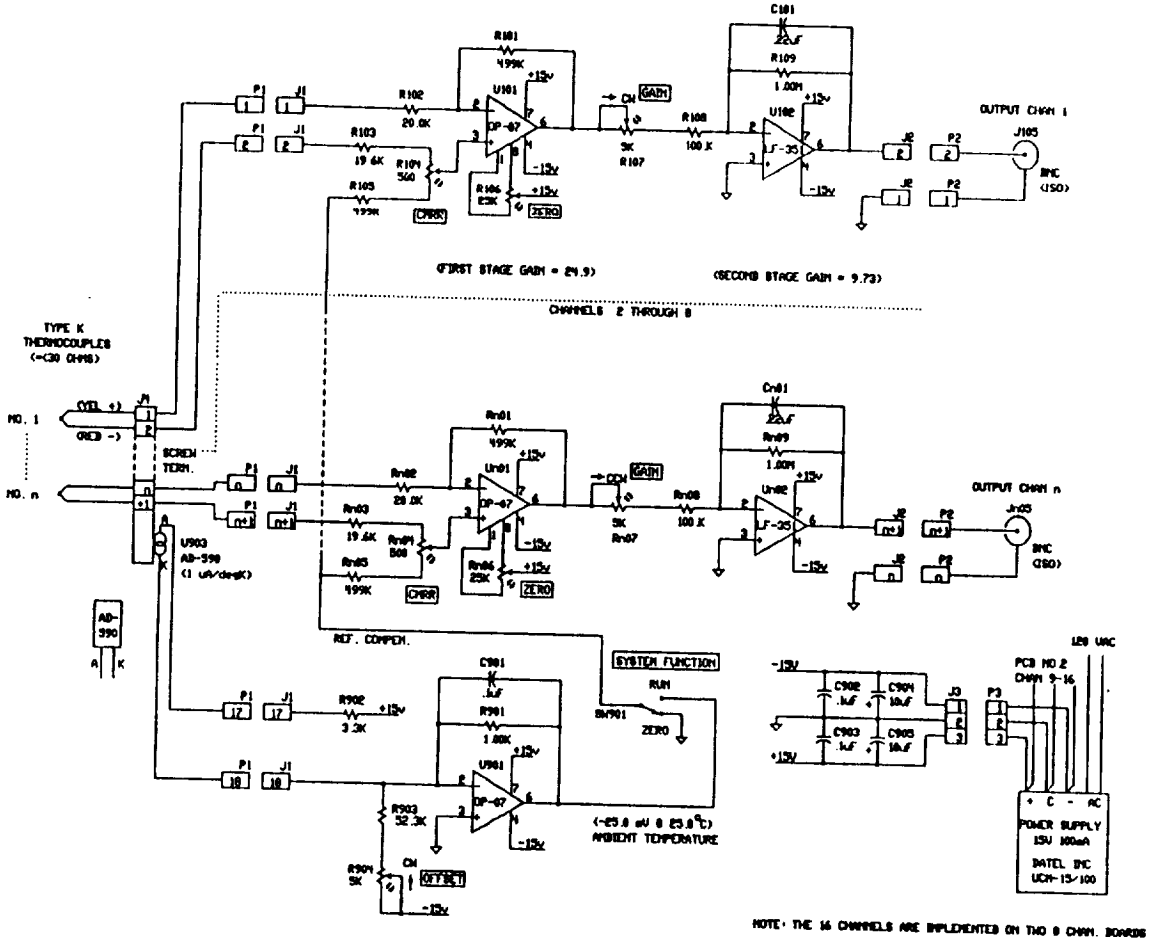

Fig. 2.6 2-stage 16-channel thermocouple amplifier with cold junction compensation.

Thermocouple interface calibration

To map the temperature of a metal conductor each thermocouple must be in good thermal, and electrical, contact with it. This causes a common mode rejection problem which is solved by the subtraction circuit of the op amps of Fig. 2.6. The voltage output is converted to temperature using the NBS algorithm for the particular thermocouple type. Calibration adjustments are made by replacing the thermocouples with a cable which connects all positive (odd number) terminals together and all negative (even number) terminals together. The reference voltage compensation is by-passed by changing jumper switches to the zero position.

Zero adjustments are made with the thermocouples shorted with a jumper cable. Potentiometers $R_{2\text{-}n}$ are adjusted to zero amplifier output.

To make the **common mode rejection adjustment**, 100 mv is applied between the shorted thermocouple inputs and the ground terminal, and potentiometers $R_{1\text{-}n}$ are adjusted to give less than 5 mv (0.5 c) at the appropriate output. The cumulative common mode error should be less than 0.5 deg c.

To adjust the **amplifier gain,** 41.27 mv is applied across the thermocouple input terminals, and the amplifier output is adjusted to 10.00 volts using trim pots $R_{3\text{-}n}$. This adjustment gives a total gain of 242.3. An output of 10.00 volts for the 41.27 mv input corresponds to the output of a type K thermocouple (chromel-alumel) operating at 1000.0 K. The amplifier gain is precisely linear. The **cold junction voltage** is provided by a temperature sensitive Analog Devices AD-590 2-terminal transistor which has a linear output current as a function of temperature.

The **cold junction compensation** is adjusted by returning the jumper switches to their normal operating position and setting the potentiometer to give an output that corresponds to the actual ambient temperature for the type of thermocouple to be used. (e.g. -25.69 mv at 25.0 C for a type K thermocouple).

Gas temperature measurement

To probe the temperature of a flowing gas T_{gas} with a thermocouple it is necessary to consider the interaction of the thermocouple with both the gas and the surrounding solid walls, particularly at temperatures where radiation from the walls and other sources is significant. The problem is to distinguish the temperature due to convective exchange with the gas from radiative exchange with the surroundings. At a steady state the sum of the heat flux components into the thermocouple is zero.

$$dq/dt = A_1 h_c (T_{gas} - T_{tc}) + A_2 k_{sb} (\epsilon_{surr} T_{surr}^4 - \epsilon_{tc} T_{tc}^4) = 0 \quad (6.1)$$

The temperature of the gas is equal to the temperature of the thermocouple minus a correction factor.

$$T_{gas} = T_{tc} - k_{sb} \epsilon A_2 (T_{surr}^4 - T_{tc}^4) / (A_1 h_c) \quad (6.2)$$

To measure a gas temperature with a thermocouple the second term of equation (6.2) must be reduced to a value small enough to reduce the error in calculating it. One approach is to reduce the difference between T_{tc} and T_{surr} by surrounding the thermocouple with multiple layers of radiation shielding. This must be done without altering the gas flow at the thermocouple. When the gas flow rate is large, a better alternative is to use the differences in the effective surface/volume ratio of the thermocouple to make the A_2/A_1 ratio small. A_2 is the physical area of the thermocouple that emits and absorbs radiation. The effective convective heat transfer area, A_1, is determined by the diameter of the thermocouple contact plus the thickness of the laminar sub-layer, δ. Assuming that the thickness of the laminar layer surrounding the thermocouple is the same as that at the walls of the flow channel and is essentially independent of the radius of the thermocouple, the ratio of areas in the heat exchange channel of the test apparatus can be calculated from the data in Tables 2.4a and 2.4b, where $\delta \approx d_h/Nu \approx .065$.

$$A_2/A_1 = \pi r_{tc}^2 / \pi (r_{tc} + \delta)^2 \quad (6.3)$$

Using 10 mil thermocouple wire, the area ratio is .16 and the correction for measurements in the heat exchange channel is as high as 80 K. The correction using 1 mil wire is about 0.5 K, which is essentially negligible.

PART III. LABORATORY RECEIVER EXPERIMENTS

Objectives of part III

(1) Define surface and volume elements of the receiver model.
(2) Measure energy flux components that are subject to independent calorimetry.
(3) Define a thermocouple array consistent with the goals of an experiment.
(4) Measure temperatures for the conditions of the experiment.
(5) Reconcile the observed temperatures with temperatures and heat flux components predicted by the model.

The object of Part III is to formulate and conduct experiments to quantify the issues inherent in generating a simple, direct representation of the major aspects of the design and performance of a particular solar receiver. The experimental data consists of temperature measurements at an array of points as a function of time after the radiation is switched on. The model allows these temperatures to be interpreted in terms of the magnitude of heat flow due to specific competing processes. Both the time dependence of the change in temperatures and the steady state values of the temperatures contribute to a correct interpretation.

The small scale receiver cannot perform as an ideal fluid absorption receiver for reasons that are explained. However experimental measurements to adjust and verify the properties of the small scale model eliminate many uncertainties in modeling and designing apparatus at a scale which allows more ideal performance.

CONTENTS OF PART III

1. TEMPERATURE DISTRIBUTION MODEL

Temperatures probe the performance of the receiver, but not directly in terms of the processes that cause it. The observed temperatures are interpreted by comparing them with temperatures resulting from the time dependent calculation described in Part I. Each element of the model and corresponding apparatus is characterized by location, size, material properties, and temperature. Elements of the small receiver model are shown in Fig. 3.1. The k-index gives axial locations. The j-index gives radial locations according to the nature of the element. The temperature, $T_{j,k}$, of each element changes as it exchanges heat components $P_{i,k}$ with adjacent elements by each of several processes, i.

Calculation procedure

Initial values - Initial values are entered for gas partial pressures, electric heater power, total radiant power, linear gas flow velocity, initial time increment, initial temperature distribution, and cooling water mass flow rate. The initial temperatures are normally set at the ambient temperature, in which case the calculation mimics the changes during an experiment from a cold start. Except for the temperatures, the initial values remain constant during a calculation. The total radiant power, total electrical power, and gas velocity can be changed on command, as might be done during an actual experiment.

Physical constants - The calculated power component for each process of each element require a constant heat exchange cross section for each interacting pair of elements multiplied by a coefficient such as the thermal conductivity of the material. Coefficients are calculated for a typical steady state temperature. The calculated temperature of each model element requires the constant heat capacity (J/deg) for each element. The heat capacity of each solid element is its measured mass times specific heat. The heat capacity of each gas element is the product of its calculated volume, density, and specific heat.

Power components, $P_{i,k}$ - The first step of the iteration is to calculate the heat flow power components. In general the heat flow at each element of the model is resolved into radial and axial components. The processes chosen for the model include at least one radial and one axial process for each element, which not necessarily the same kind of process. The is limited to the processes considered to be most significant.

Fig. 3.1 Identification of the elements of the 500 watt receiver model.

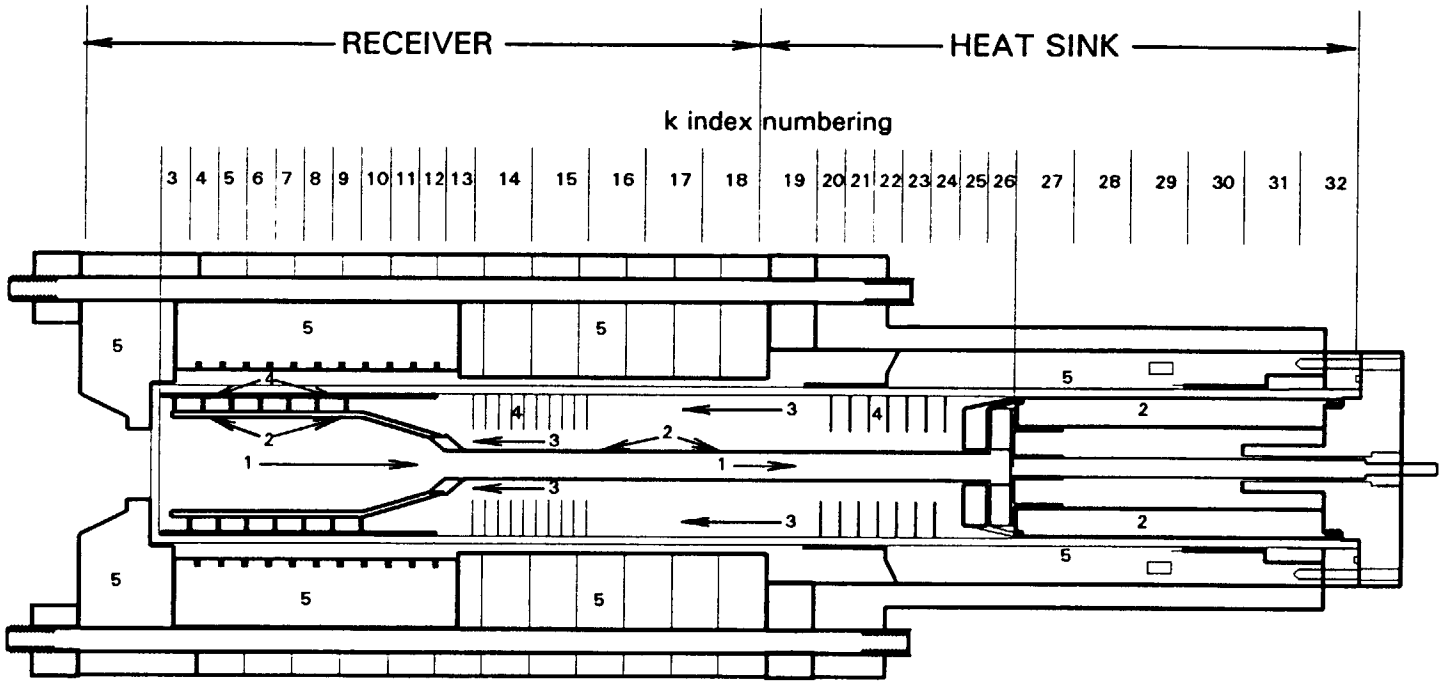

j-index (k)

1 gas out (3-26)

2 receiver (4-12)
exit tube (13-24)
blower shroud (25)
blower (26)
blower base (27-32)

3 gas in (3-26)

4 receiver hx (3-13)
radiation shields (14-15)
cold hx (20-26)

5 insulation (1-18)
barrier (19)
heat sink (20-32)

Temperature changes, $dT_{j,k}$ - The temperature change of each element over time, dt, is incremented by adding ΔT = psum(j,k)/kx(j,k), the algebraic sum of the power components into the element divided by the heat capacity of the element. The heat capacities of the elements are calculated and stored as constants. Each temperatures, $T_{j,k}$, is by definition the temperature at the center of mass of the element. For metallic elements no distinction is made between the temperature at the center of mass and the temperature of the surfaces. Radial heat flow through insulation is between an inner temperature, the temperature of the nearest metallic component, and an outer temperature at the ambient air interface. The thickness for axial flow between elements of the same material is the distance between the centers of mass of the elements.

Time increment, dt - When the initial condition is far from a steady state the calculation can exhibit instability due to the "stiffness" of the equations. An initial time increment that is too long may cause changes during a single iteration that overshoot enough to cause regenerative oscillation. A time interval short enough to avoid instability during fast changes may require so many iterations that significant truncation errors accumulate. Using the Gear methodology, instability is avoided by adjusting the iteration time interval to suit the current rate of change and/or correcting the power increments using higher derivatives of the rate of change. As long as care is used to meet the conservation conditions described below, moderate errors in the initial portion of the relaxation do not affect the accuracy of the final steady state values.

Assumptions, limitations, and tests

At the outset theoretical rigor is less important than simplicity. Some complex parallel combinations of processes are represented by a single dominant one with the proviso that the correct effective rate coefficient might represent an empirical composite of processes. The following discussion of individual processes outlines the internal checks on the self consistency of the model and lists the approximations as an aid in identifying areas that require greater rigor or further interpretation based on experiment.

Energy conservation - At the start of the relaxation most of the power input is used to heat the elements to their steady state temperatures. At the steady state the sum of the input power components must exactly balance the sum of the output power components. For this to be true every element must have a thermal path to the heat sink cooling water or to the ambient air, and every increment of power that is lost by one element must be gained by another element. The calculations of the power components are grouped as follows to facilitate energy conservation tests to verify the internal consistency of the calculations.

Fluid heat exchange and transport

P(1,k), k = 3,12	**fluid absorption power input**
P(2,k), k = 4-26	**radial convection, output gas to receiver core**
P(3,k), k = 25-3	**radial convection, return gas to heat exchangers**

The fluid gains or loses heat by fluid absorption and by convection with adjacent surfaces. In addition it transports heat by fluid flow. Each heat component represents the heat exchanged with all of the gas flowing though the gas volume element in time dt. The mass flow rate of the gas is designed to be large enough to make the total heat capacity of the gas comparable to solid elements in spite of the large discrepancy between their static heat capacities of the gas volume elements. Heat transport by the gas flow is taken into account by calculating gas temperatures in sequence in the flow direction. During each iteration the temperature of each gas element is calculated as the temperature of the previous element in the flow stream plus the change due to fluid absorption or convection starting and ending with the element nearest the window.

P(1,k) - The fluid absorption components, which are constant during an experiment, are derived from measurements and calculations described in Section 3.2 based on the bromine pressure and the total radiant power. The temperature change of the gas is calculated in two steps, first the change due to fluid absorption, then the change due to convection.

P(2,k) - Convective heat transfer by the outlet gas is calculated using the same heat transfer coefficient as the heat exchangers. The high torque output of the blower causes the gas to flow at the outer diameter of a helical channel at about the same linear flow velocity as the gas in the heat exchangers.

P(3,k) - Convective heat transfer in the heat exchangers uses the heat transfer coefficient derived in Part I. The helical side walls of the flow channel in both the hot and cold heat exchangers rely on thermal radiation for equilibration. The effective heat exchange area of the cold heat exchanger includes the surfaces of the blower and its shroud in addition to the heat exchanger helix. These surfaces also rely primarily on thermal radiation for heat flow. The more stationary gas at the center of the cold hx helix insulates the active flow gas from the hot outlet tube. The cold hx helix is designed to be trimmed empirically to give the desired return flow temperature.

Test: Run the model with processes i = 1-3 active. After 5-10 minutes set the fluid absorption, P(1,k), to zero and continue the integration. At a steady state all T(j,k) are constant and all P(i,k) are zero.

Electrical power input and insulation heat loss

P(4,k), k = 1, 3-13	**electrical power input**
P(5,k), k = 1, 3-13	**radial conductivity, insulation**
P(6,k), k = 1-18	**radial convection, insulation to ambient air**
P(7,k), k = 3-13	**axial conductivity, hot hx shroud**
P(8,k), k = 1-18	**axial conductivity, insulation**

P(4,k) - Auxiliary electrical power is used to offset the excessive heat losses that are unavoidable in a small apparatus. Measurements of the heat distribution from the electrical power input are described in Section 3.3. The electrical power input components are constant except for changes on command.

P(5,k) - Radial heat flow into the insulation, a complex combination of radiative, convective, and conductive exchange, is represented in the model by the conductivity between the inner surface at T(4,k) and the outer surface at T(6,k), where the temperature of the inner surface is the temperature of the nearest metallic component. The quartz containment is treated as an inner layer of insulation. T(5,k), the temperature at the center of mass at radius $r_c = [\frac{1}{2}(r_o^2 + r_i^2)]$, is the temperature due to the conductivity across T(4,k) -T(6,k). The general relation for radial heat flow through a cylinder, $2\pi\kappa x\ \Delta T = \ln(r_2/r_1)$, is used to calculate the temperature of the outer surface, T(6,k) = T(4,k) - 1.414 [T(4,k) - T(5,k)].

P(6,k) - Radial convection to the ambient air is calculated as convective heat exchange across temperature difference $\Delta T = T(6,k) - T_{ambient}$. The heat transfer coefficient is assigned an empirical value consistent with the observed value of T(6,k) at the steady state.

P(7,k) - Axial conductivity of the hot heat exchanger shroud redistributes heat on the inside of the insulation among elements that are not heated directly.

P(8,k) - Axial redistribution of heat in the insulation is confined to the range from the space between the front insulator and the aluminum heat barrier, element 5,19, that separates the insulation (heat loss) from the heat sink (heat load).

Tests:

(1) Run the model with processes i = 4-6 active. At any time $[P(4,k)] \geq P(5,k) \geq P(6,k)$. At a steady state $P(4,k) = P(5,k) = P(6,k)$.

(2) Run the model with processes i = 4-8 active. At a steady state $\Sigma P(4,k) = \Sigma \Sigma P(5,k) = \Sigma P(6,k)$.

(3) Run the model with processes i = 1-8 active. At a steady state (10 hours) - $\Sigma P(2,k) = 0$; $\Sigma[P(1,k) + P(2,k)] = \Sigma P(5,k) = \Sigma P(6,k)$

Direct absorption power - heat flow to the heat sink

P(9,k), k = 3-12	**direct absorption power input**
P(10,k), k = 4-32	**axial conductivity of the central core**
P(11,k), k = 20-29	**axial conductivity of the heat sink**
P(11,k), k = 32-29	**axial conductivity of the heat sink**
P(12,k), k = 14-18	**radial radiation, cold hx to heat sink**

P(9,k) - The direct absorption components of the total radiant power are based on the calorimetric measurements and calculations described in Section 3.2. The total radiant power, which is constant except for switching on command, is measured with a copper block calorimeter. The spatial distribution of the total radiant power among the receiver elements is measured using a segmented calorimeter. When bromine is present, the radiation to each receiver element is distributed between elements of the gas absorber and elements of the direct absorption receiver surface by integrating the absorbance over all wavelengths as a function of distance from the window.

P(10,k) - Axial flow from the receiver to the end cap is an unbroken conductive path except for the small fluid gap between the rotor and its bearing. Heat flow across the fluid gap, which occurs both by radiative exchange and by convective heat exchange, it treated artificially as conductivity subject to empirical adjustment. Heat flows from the end element of the central core to the end element of the heat sink to the coolant.

P(11,k) - Axial conductivity of the heat sink carries heat to element 5,29, where it is transferred to water which enters the heat sink at ice temperature at a measured flow rate. T(6,29) is the calculated temperature of the water leaving the heat sink after heating by components P(5,28) and P(5,30). The calculated cooling water temperature difference is then $P(11,k) / c_w v_w$.

P(12,k) - Radiation from the return gas heat exchanger to the heat sink is a conservative estimate of the heat transferred to the heat exchanger.

Tests:

1. Run the model with all processes except i = 4-8.
   $\Sigma [P(1,k) + P(9,k)] = P(11,28) + P(11,30)$
2. Run the model with all processes.
   $\Sigma [P(1,k) + P(4,k) + P(9,k)] = P(11,28) + P(11,30) + \Sigma P(6,k)$

Heat redistribution in the receiver

P(13,k), k = 4-12	**radiative exchange inside the receiver**
P(14,k), k = 4-9	**radiative exchange, receiver and hot heat exchanger**
P(15,k), k = 10-14	**radiative exchange, receiver-hot hx- heat shield cavity**
P(15,k), k = 14-15	**axial radiation, heat shields**
P(15,k), k = 20-26	**axial radiation, cold heat exchanger**
P(16,k), k = 26-30	**radial radiation, base to heat sink**

P(13,k) - Radiative exchange inside the receiver is calculated by redistributing the sum of the radiant power from all elements inside the receiver to each element according to its area. The exposed surface of the front insulator is included. Thermal radiation by the stainless steel surfaces is large at the higher temperatures. In the absence of adequate data the emissivity/reflectivity, $\epsilon = 1 - \rho$ of corrosion treated stainless steel is an empirical parameter.

P(14,k) - Radiative exchange between the receiver and the hot heat exchanger is calculated by redistributing the total radiation in proportion to the exposed surface areas. Since the spiral barrier in the hot heat exchanger does not have a firm thermal connection to either the receiver or the heat exchanger shroud, its temperature, maintained by radiative exchange, is taken as that of the shroud.

P(15,k) - Radiative exchange in the cavity between the receiver, the hot heat exchanger, and the radiation shield is calculated by redistribution the total radiation among those elements according to their area. The changes in the receiver elements are combined with P(13,k).

Axial flow of radiant power through the n heat shields is calculated from the relationship $P(15,14) = P(15,15) = \sigma_{SB}\, \beta\, [T(4,15)^4 - T(4,14)^4] / (n-1)$ where $\beta = (1-\rho)/(1+\rho)$ is an emissivity factor that is a function of the reflectance of the shields. T(4,14) is the temperature of the first shield. T(4,15) is the temperature of the last shield. The input radiation is subtracted from the total radiation used in calculating P(14,k). Radiation emerging from the last heat shield is distributed among elements of the insulation and the input coil of the cold heat exchanger.

The axial flow of radiant power, P(15,k) through the helical coils of the cold heat exchanger to the base of the blower is calculated as another set of heat shields. Since there are alternative inputs and outputs to each surface, the axial radiant energy exchange is taken to be independent of the other heat flow components, The total number of heat shield cavities includes the number of turns of the helix. In addition to adjustments that might be required to make the model correspond to observation, the number of turns of the helix is physical adjustment which changes the temperature of the return gas.

Radial radiation from the blower base to the heat sink, P(17,k), is calculated for the temperature difference T(2,k) - T(5,k).

2. RADIANT POWER CALIBRATION

The boundary conditions for the disposition of power in the receiver system are determined by independent measurements and related calculations. This section describes experiments to determine the total radiant power and the distribution of radiant power from the xenon arc source.

Total radiant power

The total radiant power is measured with a copper block calorimeter with a copper-constantan thermocouple attached. The 3.8 cm diameter matches the aperture of the cone collector. The mass, m, is chosen to make the exposure time long enough for accurate time measurement, but short enough to minimize the heat loss indicated by temperature nonlinearity with time. The receiver cavity is a polished 60° conical recess coated with ultrablack paint, and insulated by Cotronic ceramic paper insulation. The thermocouple voltage is measured as a function of time using the apparatus described in section 2.6. The time dependence is used to correct for heat losses as described in section 3.2.

$$\Phi_{rad} = 4.183\ m\ c_p(Cu)\ \Delta T / \Delta t \qquad \text{watts} \tag{3.1}$$

The following temperature dependent value for the specific heat of copper is derived from the molar hear capacity given by the JANAF Tables.

$$c_s = 4.183\ [5.845 + .00202\ [T(K) - 298)]\ /\ 63.54 \qquad \text{watts/g-K} \tag{3.2}$$

The calorimeter mass, m = 265.5, is small enough high temperature sensitivity and response fast enough to avoid large heat losses, but large enough for reasonably long exposures without overheating. Data for a typical measurement of the power are given in Table 3.2a. The data show that about 3.5 sec is required for the temperature in the copper block to equilibrate. The rate of heat loss measured at the end of the exposure is almost negligible, even at the highest temperature. The power is taken to be the average over the 2 sec intervals during the constant part of the temperature rise. The $\pm 3\%$ uncertainty in the power is attributed equally to the inaccuracy of the measurement and

the instability of the lamp. The current-voltage characteristic of the xenon arc is not constant. At a given current the current/voltage ratio may vary by 5-10%, but the radiant/electrical power ratio varies by about 2%.

Table 3.2a Measured values of the total radiant power as a function of time during a typical determination.

t(sec)	T(K)	power	
0	307.3	0.0	shutter opened
2	308.7	74.9	
4	316.9	417.2	
6	328.2	582.7	
8	338.8	550.3	
10	349.7	565.0	
12	360.4	558.5	
14	370.9	550.1	
16	381.7	566.7	
18	391.9	537.4	
20	403.1	596.5	
22	413.0	524.1	shutter closed
24	419.9	366.6	
26	421.1	65.0	
28	421.1	0.0	
avg		559.0 ± 16.6 watts	

Radiant power input distribution

The radiant power distribution is measured with somewhat less absolute accuracy by a calorimeter consisting of a set of isolated copper rings. Except for the insulation between rings each ring corresponds in size and location to a surface element of the model. The rings are weighed individually and mounted on a frame with insulation between rings. The temperature is measured as a function of time from the start of exposure using the same apparatus and procedure as the total radiation measurement. The

response, $\Delta T/\Delta t$, to the radiant power into each ring depends on the mass and specific heat, $c_p(Cu)$, as in equation (3.1). The thermocouple voltage of each segment is transferred to the computer at 2 sec intervals during a total exposure of 15-20 seconds, measured by the computer clock. The apparent radiant power at each ring is calculated as a function of time at 2 second intervals as in Table 3.2a. Heat loss due to radiation is is proportional to the area and fourth power of the absolute temperature, and accounts for almost half of the apparent power change during a measurement. Additional systematic changes in the apparent radiant power depend on the temperature difference between adjacent elements. The correct power components are taken to be the values extrapolated to zero time. These values are reproducible within 1 watt at each element and within 1 watt total over all elements. The best values are taken to be those obtained with the calorimeter surfaces blackened to approximate a black body. The actual receiver surface is expected to tend more toward black body emissivity as the temperature increases. The calculated relaxation time for heat to circulate from one side of the copper ring to the other is about 1 sec. Data were taken with the assembly rotated at different angles along the optical axis to show that heating the rings unsymmetrically is not a significant source of error. The distribution obtained is shown in the first column of Table 3.2b.

Table 3.2b Observed radiant power input, $\Phi_{tot}(k)$, and the calculate direct absorption and fluid absorption components for a system containing 50 torr bromine.

k	$\Phi_{tot}(k)$	$\Phi_{direct}(k)$	$\Phi_{fluid}(k)$
3	76.50	62.71	13.79
4	71.50	57.93	13.57
5	65.50	52.59	12.91
6	60.00	47.83	12.17
7	55.00	43.59	11.41
8	49.00	38.66	10.34
9	38.00	29.86	8.14
10	31.00	24.27	6.73
11	31.00	24.19	6.81
12	22.50	17.51	4.99
sum	500.00	399.14	100.86

Fluid absorption power distribution

To calculate the fluid absorption power delivered to each gas element in the receiver the total radiant power is first divided into a set of rays, j, originating at the rms radius of the window and terminating at the back each edge of each element of the inner surface of the receiver. The radiant power of each ray as it enters the receiver, $\Phi(k_{max},j)$, is the power measured with the ring calorimeter, that is, the power reaching receiver element $k = j$ in the absence of an absorber. The length of each ray, measured along the edge of the truncated cone, is divided into a set of distances, x(j,k), the distance along ray j from the window to the back of gas element k. $\Phi(k,j)$ is the power at the back edge of any gas element through which ray j passes. The total radiant power measured by the block calorimeter is the sum over all rays.

$$\Phi_{tot} = \sum_j \Phi(k_{max},j) \tag{2.3}$$

In a system containing bromine at molar concentration, m, the direct absorption component of radiant power measured at $j = k$ is the fraction of the total radiant power transmitted through the distance $x(k_{max},j)$ to element j. Since the transmittance is a function of wavelength each ray is summed over all wavelengths, n, to obtain the power measured by one element of the ring calorimeter.

$$\Phi_{dir}(j) = \sum_n \Phi(k_{max},j,n)\ 10^{-a(n)\ x(kmax,j)\ m}\ \delta n \tag{2.4}$$

For $k \leq k_{max}$, equation (2.4) is the power absorbed from ray j at depth k into the receiver. The fluid absorption power component into each gas volume element, k, is the sum over all rays of the power absorbed by that volume element, that is, the difference in the radiant power as it enters and leaves the element.

$$\Phi_{fluid}(k) = \sum_j \sum_n \Phi(j,k,n)\ [1 - 10^{-a(n)\ x(j,k)\ m}]\ \delta n$$

$$- \sum_j \sum_n \Phi(j,k,n)\ [1 - 10^{-a(n)\ x(j,k-1)\ m}]\ \delta n \tag{2.5}$$

Fig. 3.2 compares the direct absorption (upper curves) and fluid absorption (lower curves) power distribution as a function of the distance from the window at bromine concentrations ranging from 25 to 100 torr. The vertical lines mark the boundaries of the

model elements. The fraction of the radiation that is absorbed ranges from f = .174 at 25 torr (lightest curve) to f = .222 at 100 torr (heaviest curve). The increase in the fraction absorbed with bromine pressure diminishes rapidly in this pressure range. The bromine concentration needed to reach this plateau decreases with increasing scale of the receiver.

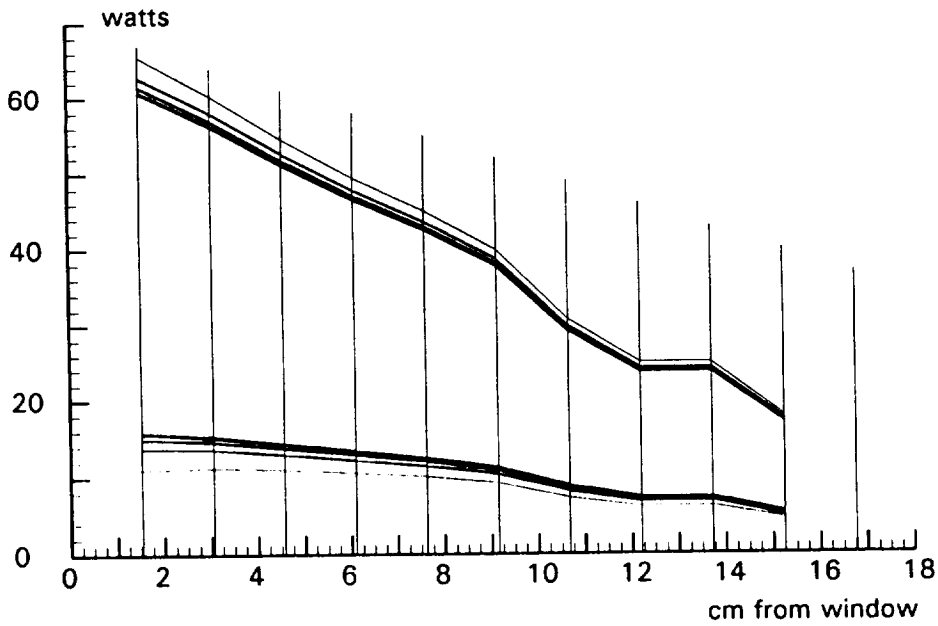

Fig. 3.2 Power absorbed by the fluid (lower curves) and power absorbed by the receiver surface (upper curves) as a function of depth in the receiver at various bromine concentrations.

It is clear from Fig. 3.2 that the distribution of direct absorption power on the receiver surface is far from the ideal uniform distribution. The cone that concentrates the input radiation also increases the angle at which radiation leaves the cone. The distribution is a compromise that maximizes the irradiance of the radiation input, makes the irradiance at the receiver surface comparable to the thermal irradiance at the operating temperature of the receiver, and makes the receiver surface area compatible with the requirements for convective heat transfer.

3. HEAT LOSS CALIBRATION

The thickness of the insulation required to produce a given temperature difference is independent of the size of the apparatus. The heat content of insulation required to reduce heat loss from a small receiver to a small fraction of the radiant power input is large enough to give a small system great thermal inertia. It requires more than 100 watt-hours to heat the insulation in Fig. 3.1 to the steady state temperature with the receiver at 1200 K. As an alternative the laboratory receiver is surrounded by a radiant heater which compensates for the heat loss that would otherwise be prevented by more effective insulation or radiation shielding. In doing this the measured electrical power delivered to the furnace becomes a useful way to calibrate the heat loss distribution.

When the receiver is heated by the radiant heating coils with no gas flow it reaches a high temperature steady state at which the power input is balanced by power loss through the insulation. This isolates the heat loss, primarily thermal conductivity of the insulation, from competitive heat exchange processes. When the heater input power is adjusted to give the required receiver temperature without flow, the heater power is a clearly defined part of the insulation power loss under dynamic flow conditions.

Insulation heat loss distribution

To measure the insulation heat loss distribution the apparatus is insulated as shown in Fig. 3.1. In addition the input aperture is closed with a ceramic foam plug. Temperatures are monitored at several points inside the cavity, the front cover plate, the furnace sides, the outer insulation casing, and the heat sink. The receiver filled with argon without flow. When a calibrated power is applied to the heater a steady state is reached in 1-2 hours with the center of the furnace at T_{max} = 1200 K. The measured electrical power input is then equal to the heat loss through the insulation. The distribution of that heat loss is inferred from the measured temperature differences using the manufacturer's value for the thermal conductivity of the insulation. Sample results using a preliminary apparatus configuration are summarized in Table 3.3a.

Table 3.3a Preliminary measurement of the power loss from a closed receiver cavity containing argon heated to 1200 K by 315 watts electrical power with no flow. The loss is calculated from the measured temperatures using κ_{ins} = .0013 watts/cm-K for the thermal conductivity of the insulation.

T(K), in	T(K), out	watts	location
1189	764	8.8	center, front end plate
1189	715	9.8	edge
1189	425	44.7	furnace front
1202	414	46.1	
1202	414	46.1	
1202	413	46.2	
1202	413	46.2	
1190	416	45.3	furnace rear
1190	467	15.0	center, rear end plate
1190	575	12.8	edge
		321.0	

The power calculated from the thermal conductivity of the insulation agrees with the measured total power within the ambiguity in the effective insulation thickness due to the imbedded heating coils. Both the inside and outside temperatures are reproducible. The temperature coefficient of the electrical heater power is about 1 watt/degree.

The calculated heat loss assumes that there is good thermal contact among all of the components in the hot cavity. At 1200 K the total the thermal radiant power exchanged by all surfaces inside the furnace is more then an order of magnitude greater than the electrical power input. When the furnace contains a tube similar to the receiver, there is no detectable change in the steady state power distribution from the empty cavity at the same temperature. This would be expected if the contents of the cavity, including the inner surface of the insulation, are near their black body emissivities, $\epsilon = 1$. In this approximation the quartz tube and surrounding gas layers are treated as if they were a an inner layer of the insulation.

Heat loss by re-radiation through the input aperture

When the measurement described above is repeated with the front end insulation plug replaced by the radiation input aperture with its associated insulation. The major difference from this replacement is the large, known component of 1200 K radiation from the inlet aperture. Changes in the details of the insulation configuration at both the aluminum collector cone and the rear end of the cell account for some of the differences in the power loss distribution. The radiation loss through the inlet aperture is calculated for a black body at 1200 K.

Table 3.3b Preliminary measurement of the heat loss distribution from the insulation plus the front inlet aperture. The steady state cavity temperature of 1200 K require 515 watts of electrical power.

T(K), in	T(K), out	watts	location
1148	-	134.0	radiation out
1148	782	34.1	center, front end plate
1148	567	16.0	edge
1148	410	43.2	furnace front
1169	399	45.1	
1169	399	45.1	
1200	402	46.8	
1200	402	46.8	
1197	398	46.3	furnace rear
1197	483	7.4	center, rear end plate
1197	537	20.5	edge
		499.9	

The 15 watt discrepancy between the measured power input and the heat loss calculated from thermal conductivities suggests and additional source of power loss. A further measurement described below suggests that free convection inside the entry cone may account for the difference.

Temperature measurements in strong radiation

In the absence of radiation thermocouples inside the receiver have only minor deviations from the central black body temperature. These are attributable to the known end effects. With the light source on, thermocouples in the radiation input aperture deviate from the central cavity temperature in ways that are attributable to the non-isotropic nature of the radiation. The following experiment examines this more quantitatively. A thermocouple is attached to a stainless steel disc with area A = 1 cm^2 which is placed in the aperture facing the radiation. At a steady state the front side of the disc absorbs the input radiation while the back side absorbs thermal radiation from the cavity at temperature $T_{cav.}$ Both sides of the disc emit thermal radiation at the temperature measured by the thermocouple, T_{tc}.

$$\epsilon_{tc}\,\Phi_{tot} + \sigma\,\epsilon_{tc}\,A\,T_{cav}^4 = 2\,\sigma\,\epsilon_{tc}\,A\,T_{tc}^4 \qquad (2.6)$$

The radiation terms are measured or calculated from measured temperatures. Although the emissivity of the thermocouple disc appears in all of the radiation terms, its spectral distribution might be different for the xenon radiation than for thermal radiation. The power components, and associated temperatures measured with the xenon lamp off (ambient background) and on are shown in Table 3.3 c.

Table 3.3c Power components and corresponding measured temperatures associated with thermocouple readings in the non-isotropic radiation at the receiver input.

	xenon off		xenon on	
Φ_{rad}	0.14	400 K	48.2	
Φ_{rec}	11.37	1190 K	12.15	1210 K
$2\,\Phi_{tc}$	4.53	795 K	56.5	1494 K
	(7.0)		(4.2)	

The discrepancy is attributed to free convection. To test this hypothesis. the experiment was repeated using two thermocouples, one above the other. The lower thermocouple rose to the value in Table 3.3c in a few seconds. The upper thermocouple rose to a much higher temperature and melted. This is taken as proof that convective air currents are strong in the entry cone.

4. GAS FLOW CALIBRATION

The velocity of the gas is measured by the static pressure between probes normal to the gas flow near the heat exchanger input and output. The pressure drop is calibrated with the receiver attached to an external gas supply in series with a rotameter flow meter through connectors which leave the heat exchange flow path unchanged. The flow meter is calibrated by the weight loss of a small gas supply cylinder over a measured time. The pressure transducer is calibrated with reference to a water manometer. At room temperature the Bernoulli effect at each probe is identical.

To account for the effect of the range of different conditions to be used the calibration is expressed in the form of the fundamental equation for viscous pressure drop derived from basic principles in Part I, according to which the pressure change is proportional to the kinetic energy of the gas. The data for air in Table 3.4a and argon in Table 3.4b differ substantially from that calculated from that calculated using the standard equation with the Blasius skin friction coefficient, $c_f = .079\ Re^{-.25}$.

$$\Delta P = \tfrac{1}{2}\, \rho\, v_x^2\, c_f\, A_h/A_f \tag{2.8}$$

Table 3.4a Observed flow rates compared with the pressure drop in air at room temperature using $c_f = .079\ Re^{-.25}$.

v_x cm/sec	ΔP_{calc} g/cm-sec	ΔP_{obsd} g/(cm-sec	Percent difference
451	582	490	15.81
676	1182	980	17.09
901	1955	1372	29.82
1127	2892	2107	27.14
1352	3977	2744	31.00
1578	5213	3479	33.26
1803	6582	4214	35.98
2028	8086	5096	36.98
2254	9728	6076	37.54
2479	11491	6860	40.30
2704	13378	7987	40.30

Table 3.4b Observed flow rates compared with the pressure drop in argon at room temperature using $c_f = .079\ Re^{-.25}$.

v_x (Ar) cm/sec	ΔP_{calc} g/(cm-sec)	ΔP_{obsd} g/(cm-sec)	Percent difference
384	586	588	.34
577	1195	980	17.99
766	1962	1470	25.08
960	2914	2058	29.37
1149	3990	2793	30.00
1343	5243	3528	32.71
1537	6639	4410	33.57
1726	8133	5292	34.93
1920	9800	6027	38.50
2109	11550	7056	38.91
2303	13473	8085	39.99

The substantial difference between the observed values for argon and air is partly attributable to the difference in density and viscosity of the gases. The systematic change in the difference between the observed and calculated values as a function of flow rate suggests that the problem is the functional form of the skin friction coefficient. The Blasius value for c_f was determined for fully developed turbulent flow through cylindrical tubes. Flow through the heat exchanger differs in three respects. The heat exchanger channel has a small square cross section. The gas velocities are at the lower limit of turbulent flow. The flow regime is not necessarily fully developed over the full tube length. If fully developed turbulent flow requires a distance 20 times the channel width, that is about 16% of the actual channel length.

Since the uncertainties associated with the nature of the flow regime are all a function of the Reynolds number, the approach is to derive an empirical function of Re that applies to this specific apparatus. Note that the Reynolds number contains the functional dependence on the coefficient of viscosity. The density and the viscosity then encompass the temperature dependence. The function $c_f = .418\ Re^{-.481}$, derived from a least squares fit of the data in Table 2.5c, has a stronger functional dependence on Re, as expected. One test is whether this accounts for the differences between gases.

Fig. 3.4 compares the same observed data for the pressure differences as a function of flow velocity in argon and air (vertical bars) with values calculated using equation (2.8) with a skin friction coefficient $c_f = .418\ Re^{-.481}$. The modified equation accounts for both the velocity dependence and the difference in the properties of the two gases within the accuracy of the measurements.

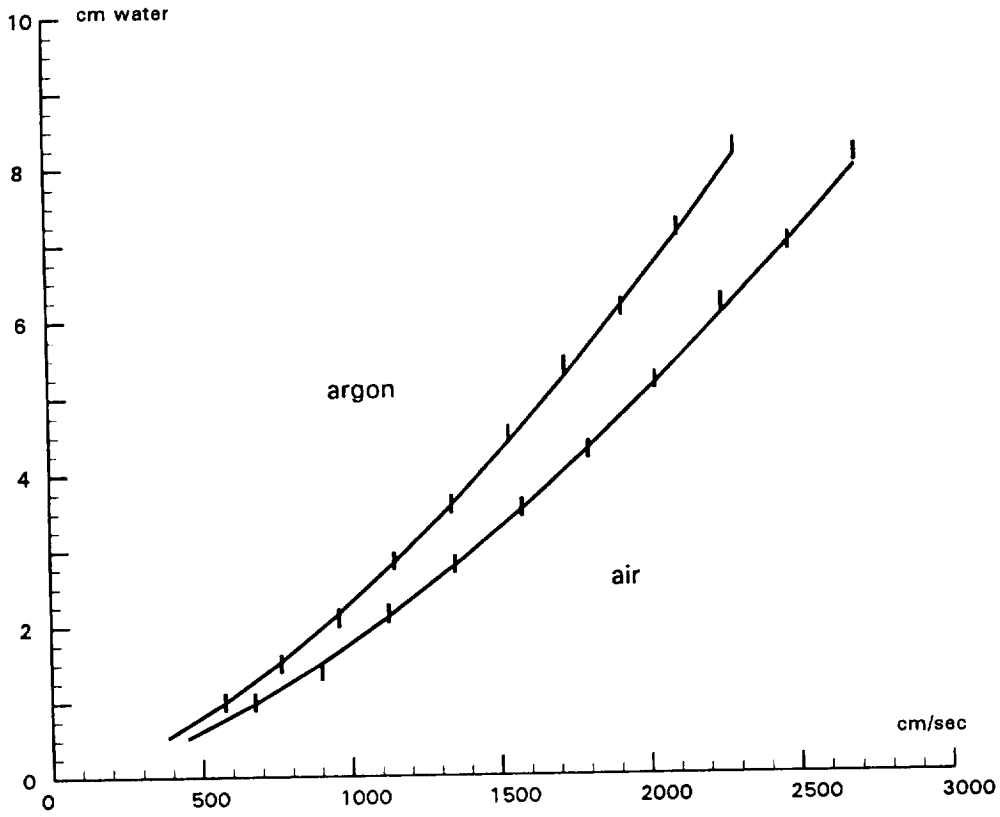

Fig. 3.4. Observed flow rates in argon and air (vertical bars) compared with the value calculated from equation (2.8) using the modified skin friction coefficient.

Gas density distribution

The local gas densities and linear flow rate depend on the local temperatures and volumes. Volume components are estimated from the dimensions of the apparatus and assigned temperatures consistent with the heat exchange properties in section 4. The results are summarized in Table 2.5d.

Table 3.4c. Calculated local gas temperature and density distribution.

location	V(cc)	T(K)	ρ(mg/cc)
window region	64	1200	.194
receiver inside	203	1200	.194
output cone and tube	108	1200	.194
convective heat exchanger	164	1020	.228
outside of hx cover	199	1020	.228
outside of blower	176	793	.294
blower shaft	141	547	.426
outside of blower support	38	547	.426
total / mean value	1092	1040	.220

The mass distribution given by the temperature/volume distribution in Table 2.5d is used to calculate the average temperature and the system pressure when it is operating at the nominal conditions. These results are used to calculate the dynamic properties in Table 2.5e.

Table 3.4d. Calculated dynamic system conditions.

system pressure	4.09	atm
average system temperature	1040	K
heat exchanger temperature	1020	K
heat exchanger gas density, avg	2.28	mg/cc
Bernoulli effect at hx input	2.18	torr
Bernoulli effect at hx output	1.72	torr
heat exchanger pressure drop	8.33	torr

5. STATUS AND CONCLUSIONS

The preceding report describes the development of a solar receiver and a computer model of its performance as an integrated interactive process. As noted on page iii of the introduction, this is a progress report on the status of work that is continuing under other auspices. A progression of versions of laboratory scale test apparatus components has resolved many of the critical issues. Two issues involving the gas circulation blower have delayed a full operational test of the complete apparatus. Nevertheless the calibration tests which have been the basis for revisions provide some confidence that the model described in section 3.1 is a useful first approximation to the actual performance. The purpose of this section is to show how the calculated data for the small scale test receiver is related to questions that might be answered by continuing the course outlined in the introduction.

Table 3.5 shows the calculated temperatures in the test apparatus with and without bromine absorber under the nominal operating conditions and receiver specifications defined in Part II. The blank line after k = 18 separates the receiver from the heat sink. The differences in these two cases are consistent with the predictions of more limited calculations in Part I. The maximum receiver-hx temperature is 14° above the gas outlet temperature when the system contains bromine, but 95° above the gas outlet temperature when the system contains only argon. In both cases the gas enters the hot heat exchanger at about 600 K and is heated to about double that temperature in the heat exchanger. The temperature of the gas containing bromine continues to rise. The temperature of the gas containing no absorber decreases monotonically. The gas leaves the receiver at about the same temperature in both cases. Before concluding what this distinction says about the relative merits of the fluid absorption process it is necessary to consider the limitations imposed by the small scale of the laboratory apparatus.

The fraction of the radiant power absorbed by the gas will be larger in a field test apparatus due to the improved spectral distribution of solar radiation over the xenon arc. The bromine concentration can be much smaller and the absorbed power can be distributed over greater depth due to the increase in absorption path. Using bromine as the absorber, the fluid absorption effect will be enhanced by at least 30%.

Table 3.5 Temperatures predicted by the preliminary model program

a) argon with added bromine absorber

k	gas out	center core	gas in	hx	ins/ sink	ins out
1				1171	411	329
2					388	310
3	1241		1221	1238	434	347
4	1253	1221	1183	1199	442	354
5	1260	1213	1150	1170	445	356
6	1263	1200	1108	1134	445	356
7	1262	1185	1052	1088	443	354
8	1256	1170	977	1031	441	353
9	1247	1157	862	979	441	353
10	1242	1155	611	1048	445	356
11	1242	1156	611	1069	454	363
12	1242	1154	611	1073	470	376
13	1236	1147	611	1070	504	403
14	1230	1184	611	898	578	462
15	1228	1211	611	390	431	345
16	1227	1219	611		389	311
17	1226	1219	611		378	303
18	1224	1211	611		376	301
19	1220	1189	611			
20	1217	1162	611	594	344	
21	1211	1122	647	626	341	
22	1202	1058	691	665	335	
23	1188	959	747	712	333	
24	1165	803	821	773	330	
25	1129	555	923	852	326	
26	1074	546	1074		319	
27		527			313	
28		490			306	
29		453				290
30		417			302	
31		380			304	
32		343			306	

b) argon with no absorber

k	gas out	center core	gas in	hx	ins/ sink	ins out
1				1218	413	330
2					389	311
3	1296		1296	1315	438	350
4	1292	1276	1249	1263	447	358
5	1286	1265	1212	1230	450	360
6	1279	1250	1168	1191	449	359
7	1270	1233	1109	1142	447	358
8	1259	1214	1026	1078	445	356
9	1247	1199	895	1017	445	356
10	1239	1196	593	1086	450	360
11	1235	1197	593	1107	459	368
12	1231	1194	593	1110	479	383
13	1228	1182	593	1107	519	415
14	1225	1201	593	929	607	485
15	1224	1214	593	404	439	351
16	1223	1217	593		391	312
17	1222	1215	593		379	303
18	1220	1206	593		376	301
19	1215	1183	593			
20	1212	1155	593	578	340	
21	1206	1113	628	610	338	
22	1196	1048	671	649	332	
23	1181	948	727	697	330	
24	1157	792	801	759	328	
25	1119	547	904	841	324	
26	1061	538	1061		318	
27		520			312	
28		484			306	
29		449				289
30		413			302	
31		377			304	
32		342			306	

The primary effect of fluid absorption is to redistribute the convective exchange between the receiver and the gas. In the quasi-equilibrium approximation convection, thermal conductivity, radiation, and the original radiant power input distribution tend to equilibrate the surface temperatures of the receiver surfaces. Using a dynamic model it becomes practical to ask whether there are conditions under which the output temperature of the gas might significantly exceed the temperatures of the surfaces in the receiver.

In the small scale receiver it was not practical to integrate the design of the collector and receiver optics to control the distribution of radiation in the receiver. In a field test using actual solar radiation on a larger scale, integrating the collector-receiver optical design ought to be a significant pert of the design process.

The small scale receiver offers limited possibilities to manipulate the nature of the gas flow and convective heat exchange. It is possible to contemplate circumstances under which laminar flow might use slow flowing gas as dynamic insulation of the receiver walls against the hot, faster flowing body of the fluid.

Thermal inertia, defined in this case as the time required for the calculated output power to relax to within 1% of its steady state value, is a notable feature of the test apparatus. The relaxation requires more than an hour. A larger scale can greatly decrease the relative power lost through the insulation as well as increase the options for insulating the apparatus. Thermal inertia, which is likely to be large at any scale, is intimately tied to the question of thermal energy storage and the duration of the eclipse portion of the solar radiation cycle. The ultimate design of a solar dynamic system would integrate the design of the thermal energy storage with the design of the receiver insulation or heat shielding.